

THE DEEP2 GALAXY REDSHIFT SURVEY: THE ROLE OF GALAXY ENVIRONMENT IN THE COSMIC STAR-FORMATION HISTORY

MICHAEL C. COOPER¹, JEFFREY A. NEWMAN¹, BENJAMIN J. WEINER², RENBIN YAN¹, CHRISTOPHER N. A. WILLMER², KEVIN BUNDY³, ALISON L. COIL^{2,7}, CHRISTOPHER J. CONSELICE⁴, MARC DAVIS^{1,5}, S. M. FABER⁶, BRIAN F. GERKE⁵, PURAGRA GUHATHAKURTA⁶, DAVID C. KOO⁶, KAI G. NOESKE⁶

Draft version November 2, 2021

ABSTRACT

Using galaxy samples drawn from the Sloan Digital Sky Survey and the DEEP2 Galaxy Redshift Survey, we study the relationship between star formation and environment at $z \sim 0.1$ and $z \sim 1$. We estimate the total star-formation rate (SFR) and specific star-formation rate (sSFR) for each galaxy according to the measured [O II] $\lambda 3727\text{\AA}$ nebular line luminosity, corrected using empirical calibrations to match more robust SFR indicators. Echoing previous results, we find that in the local Universe star formation depends on environment such that galaxies in regions of higher overdensity, on average, have lower star-formation rates and longer star-formation timescales than their counterparts in lower-density regions. At $z \sim 1$, we show that the relationship between *specific* SFR and environment mirrors that found locally. However, we discover that the relationship between *total* SFR and overdensity at $z \sim 1$ is inverted relative to the local relation. This observed evolution in the SFR-density relation is driven, in part, by a population of bright, blue galaxies in dense environments at $z \sim 1$. This population, which lacks a counterpart at $z \sim 0$, is thought to evolve into members of the red sequence from $z \sim 1$ to $z \sim 0$. Finally, we conclude that environment does not play a dominant role in the cosmic star-formation history at $z < 1$: the dependence of the mean galaxy SFR on local galaxy density at constant redshift is small compared to the decline in the global SFR space density over the last 7 Gyr.

Subject headings: galaxies:high-redshift, galaxies:evolution, galaxies:statistics, galaxies:fundamental parameters, large-scale structure of universe

1. INTRODUCTION

The global level (or space density) of star-formation activity has dropped dramatically from $z \sim 1$ to the present (Lilly et al. 1996; Madau et al. 1996). While measurements of the cosmic star-formation history have significantly improved in precision over the past decade (e.g., Steidel et al. 1999; Wilson et al. 2002; Hopkins 2004; Hopkins & Beacom 2006), constraining the evolution at $z \lesssim 1$ to within $\sim 50\%$, the cause of this global decline at late times is still poorly understood.

A wide variety of mechanisms, such as fuel exhaustion via the gradual or rapid depletion of gas reservoirs or the impact on star formation of a decline in the galaxy merger rate, have been considered as possible culprits for the reduction in star-formation activity since $z \sim 1$ (e.g., Le Fèvre et al. 2000; Hammer et al. 2005; Noeske et al. 2007a; Zheng et al. 2007). Many of the potential causes

for the decline in the global star-formation rate should be closely linked to the environment in which a given galaxy is found. Physical processes such as ram-pressure stripping or galaxy harassment, which preferentially occur in regions of higher galaxy density (e.g., Gunn & Gott 1972; Moore et al. 1996, 1998; Hester 2006), can remove gas from galaxies as they fall into rich groups and clusters, leading to a depletion in star formation via starvation. Heating of intracluster gas due to cluster mergers (e.g., McCarthy et al. 2007) or virial shock heating of infalling gas in massive dark matter halos (e.g., Birnboim & Dekel 2003; Kereš et al. 2005) could also be responsible for cutting off the supply of cold gas in high-density environments. Similarly, galaxy groups are the preferred location for galaxy mergers (Cavaliere et al. 1992) and interactions which may induce bursts of star formation and/or expulsion of gas (e.g., Mihos & Hernquist 1996; Cox et al. 2006; Lin et al. 2007).

The advent of large spectroscopic galaxy surveys, such as the Sloan Digital Sky Survey (SDSS, York et al. 2000) and the 2-degree Field Galaxy Redshift Survey (2dFGRS, Colless et al. 2001), has greatly enhanced our ability to study the connection between galaxies and their environments (determined from the local overdensity of galaxies). Many galaxy properties — including their star-formation rates (SFR) — have been found to depend on galaxy environment in the local Universe (e.g., Davis & Geller 1976; Balogh et al. 2004a; Kauffmann et al. 2004; Christlein & Zabludoff 2005). For instance, Blanton et al. (2005a) showed that the typical rest-frame color, luminosity, and morphol-

¹ Department of Astronomy, University of California at Berkeley, Mail Code 3411, Berkeley, CA 94720 USA; cooper@astro.berkeley.edu, jnewman@astro.berkeley.edu, renbin@astro.berkeley.edu, marc@astro.berkeley.edu

² Steward Observatory, University of Arizona, 933 N. Cherry Avenue, Tucson, AZ 85721 USA; bjw@as.arizona.edu, cnaw@as.arizona.edu, acoil@as.arizona.edu

³ Department of Astronomy & Astrophysics, University of Toronto; bundy@astro.utoronto.ca

⁴ University of Nottingham, University Park, Nottingham, NG7 2RD, UK; conselice@nottingham.ac.uk

⁵ Department of Physics, University of California at Berkeley, Mail Code 7300, Berkeley, CA 94720 USA; bgerke@astro.berkeley.edu

⁶ UCO/Lick Observatory, UC Santa Cruz, Santa Cruz, CA 95064 USA; faber@ucolick.org, raja@ucolick.org, koo@ucolick.org

⁷ Hubble Fellow

ogy of nearby galaxies is highly correlated with the local galaxy density on $\sim 1 h^{-1}$ Mpc scales.

As the SDSS and 2dFGRS have revolutionized the study of nearby galaxies, recent advances in the scope of galaxy surveys at higher redshifts have permitted some of the first studies of environment able to span a continuous range of galaxy densities from voids to rich groups and clusters at $z \sim 1$. Among the current generation of surveys, the DEEP2 Galaxy Redshift Survey (Davis et al. 2003; Faber et al. 2008) is best suited for studying galaxy environments at $z \sim 1$, thanks to its relatively large area and unmatched sample size, number density, and velocity precision.

Studies of galaxies at intermediate redshift have found that many of the global trends with environment observed locally were in place at $z \sim 1$; using the DEEP2 sample, Cooper et al. (2006) showed that the color-density relation was already well-established then, with red galaxies favoring dense environments relative to their blue counterparts and the bluest galaxies favoring underdense environments most strongly. Recent results from COSMOS (Scoville et al. 2007) and the VVDS (Le Fèvre et al. 2005) have found similar trends when looking at both the colors and morphologies of galaxies at intermediate redshift (e.g., Cucciati et al. 2006; Cassata et al. 2007).

The DEEP2 spectroscopy allows measurement of star-formation rates using the same indicator, $[\text{O II}] \lambda 3727\text{\AA}$ luminosity, over the full primary redshift range of the survey ($0.75 < z < 1.45$). Due to the high spectral resolution employed ($R \sim 5000$), this line can be detected down to relatively low star-formation rates ($\gtrsim 5 M_{\odot} \text{yr}^{-1}$ at $z \sim 1$). Of course, measurements of luminosities in the ultraviolet are sensitive to dust-extinction corrections, and the relationship between $[\text{O II}]$ and star-formation rates should also depend on gas metallicities. However, using multiwavelength data over wide fields such as the Extended Groth Strip (EGS, Davis et al. 2007), $[\text{O II}]$ line luminosities have recently been calibrated against a variety of star-formation indicators out to intermediate redshifts, testing the impact of these effects and improving the robustness of $[\text{O II}]$ star-formation rate estimates (Moustakas et al. 2006; Weiner et al. 2007).

In this paper, we utilize galaxy samples drawn from the SDSS and DEEP2 surveys to conduct a detailed study of the relationship between star formation and environment at both $z \sim 0$ and $z \sim 1$, using as closely equivalent samples and measurement techniques as possible. Our principal aim is to investigate the role of environment in the global decline of the cosmic star-formation rate space density. In §2, we discuss the data samples employed along with our measurements of galaxy environments and star-formation rates. Our main results regarding the relationship between star formation and galaxy environment are presented in §3 and §4. In §5, we detail possible sources of contamination. Finally, in §6 and §7, we discuss our findings alongside other recent results and summarize our conclusions. Throughout this paper, we assume a flat Λ CDM cosmology with $\Omega_m = 0.3$, $\Omega_{\Lambda} = 0.7$, $w = -1$, and $h = 1$ (that is, a Hubble parameter of $H_0 = 100h \text{ km s}^{-1} \text{ Mpc}^{-1}$).

2. THE DATA SAMPLES

With spectra for nearly a million galaxies, the Sloan Digital Sky Survey (SDSS, York et al. 2000) provides the most expansive picture of the large-scale structure and local environments of galaxies in the nearby Universe yet. To study star formation and its relationship with galaxy density at low redshift ($z \sim 0.1$), we select a sample of 364,839 galaxies from the SDSS public data release 4 (DR4, Adelman-McCarthy et al. 2006), as contained in the NYU Value-Added Galaxy Catalog (NYU-VAGC, Blanton et al. 2005b). We restrict our analysis to galaxies in the redshift regime $0.05 < z < 0.1$ in an effort to target the nearby galaxy population while probing a broad range in galaxy luminosity and simultaneously minimizing aperture effects related to the finite size of the SDSS fibers. In addition, we limit our sample to SDSS fiber plates for which the redshift success rate for targets in the main spectroscopic survey is 80% or greater.

In turn, the recently-completed DEEP2 Galaxy Redshift Survey provides the most detailed census of the Universe at $z \sim 1$ to date. DEEP2 has targeted $\sim 50,000$ galaxies in the redshift range $0 < z < 1.4$ down to a limiting magnitude of $R_{\text{AB}} = 24.1$. Consisting of four widely separated fields, the survey area covers ~ 3 square degrees of sky or roughly 15 times the area of the full moon, with a total of $> 25,000$ unique high-precision redshifts from $z = 0.7$ to $z = 1.4$. In this paper, we utilize a subset consisting of 15,987 galaxies with accurate redshifts (quality $Q = 3$ or $Q = 4$ as defined by Davis et al. 2007) in the range $0.75 < z < 1.05$ and drawn from all four of the DEEP2 survey fields. The redshift distributions for the SDSS and DEEP2 galaxy samples used in this paper are plotted in Figure 1.

2.1. Measurements of Rest-frame Colors and Luminosities

For both the SDSS and DEEP2 galaxy samples, we compute rest-frame $U - B$ colors and absolute B -band magnitudes (M_B) using the *kcorrect* K-correction code (version v4.1.2) of Blanton & Roweis (2007, see also Blanton et al. 2003). The rest-frame quantities for the SDSS sample are derived from the apparent *ugriz* data in the SDSS DR4, while CFHT 12K *BRI* photometry (Coil et al. 2004a) is used for the DEEP2 sample. All magnitudes within this paper are on the AB system (Oke & Gunn 1983) to the degree to which SDSS magnitudes are AB (as the DEEP2 photometry was calibrated using SDSS). For conversions between AB and Vega magnitudes, we refer the reader to Table 1 of Willmer et al. (2006).

The distribution of SDSS and DEEP2 galaxies in $U - B$ versus M_B color-magnitude space is shown in Figure 2. As found by many previous studies (e.g., Bell et al. 2004; Willmer et al. 2006), the galaxy color-magnitude diagram both at $z \sim 0$ and at $z \sim 1$ exhibits a clear bimodality in rest-frame color, with a tight red sequence and a more diffuse “blue cloud” of galaxies. We use here the same magnitude-dependent cut to divide the red sequence and blue cloud at $z \sim 1$ as employed by Willmer et al. (2006); this division in $U - B$ color is shown in Figure 2 as the dashed red line and is given by

$$U - B = -0.032(M_B + 21.62) + 1.035. \quad (1)$$

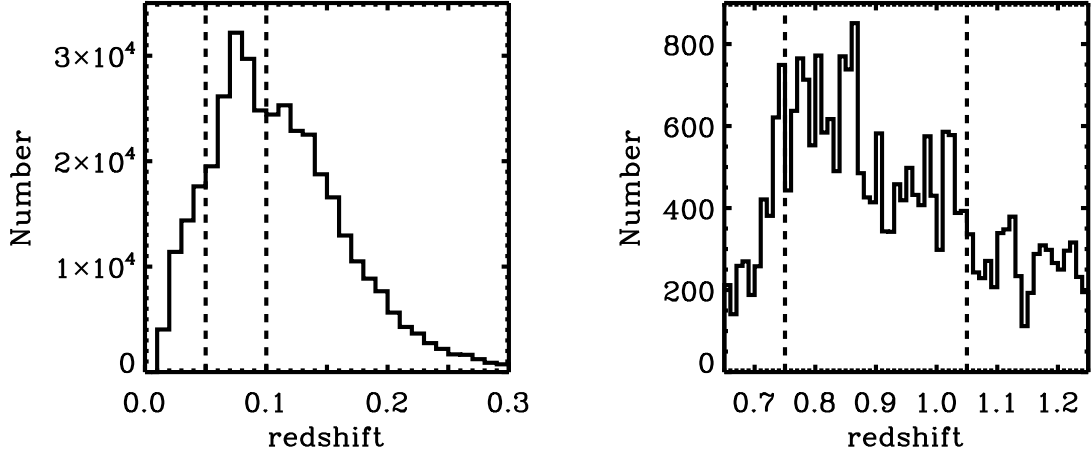


FIG. 1.— (*Left*) The observed redshift distribution for the 374,866 galaxies drawn from the SDSS within $0.01 < z < 0.3$. (*Right*) The observed redshift distribution for the 24,827 DEEP2 galaxies within $0.65 < z < 1.25$. Both redshift histograms are plotted using a bin size of $\Delta z = 0.01$. The dashed vertical lines indicate the redshift ranges within each sample used for this paper.

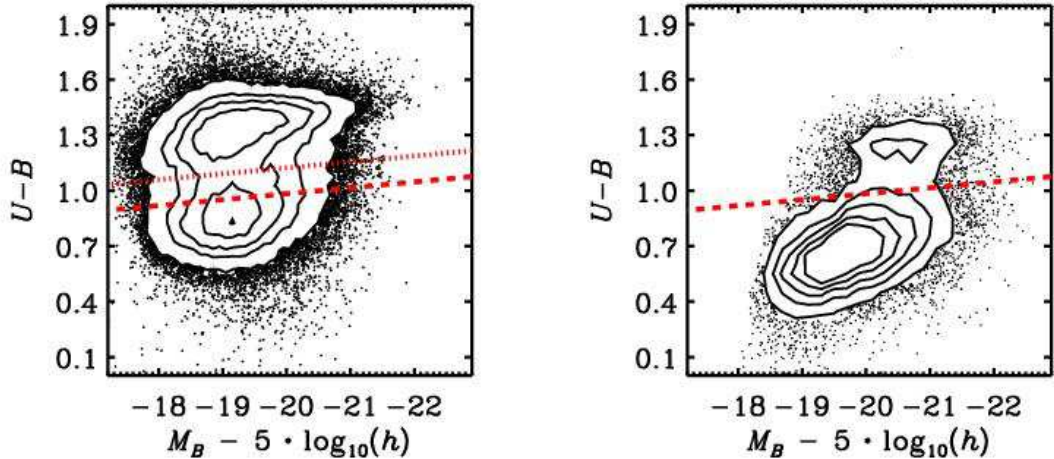


FIG. 2.— The rest-frame $U-B$ versus M_B color-magnitude distributions for SDSS galaxies in the redshift range $0.05 < z < 0.1$ (*left*) and for DEEP2 galaxies in the redshift range $0.75 < z < 1.05$ (*right*). Due to the large number of galaxies in the each sample, we plot contours (rather than individual points) corresponding to 50, 150, 250, 400, 600, and 1000 galaxies per bin of $\Delta(U-B) = 0.05$ and $\Delta M_B = 0.1$ for the SDSS, and corresponding to 50, 100, 150, 200, and 250 galaxies per bin of $\Delta(U-B) = 0.1$ and $\Delta M_B = 0.2$ for DEEP2. Outside of the lowest contour levels, the individual points are plotted. The *dashed* red horizontal line shown in both plots illustrates the division between the red sequence and the blue cloud used at $z \sim 1$, following the relation given in Equation 1. The *dotted* red line in the left plot is shifted relative to the dashed line by $\Delta(U-B) = 0.14$.

For the SDSS sample, the red sequence is shifted redward relative to that of the DEEP2 data by approximately 0.2 magnitudes in $U-B$ color (cf. Fig. 2 and Blanton 2006). This shift is consistent with the predicted evolution of an old, passively evolving stellar population, which should redden in $U-B$ color by ~ 0.14 magnitudes from $z \sim 0.9$ to $z \sim 0.1$ (van Dokkum & Franx 2001). The dotted red line in Fig. 2 is simply the DEEP2 division (given by Equation 1) shifted by $\Delta(U-B) = 0.14$; it provides a relatively clean divide between the red sequence and blue cloud at $z \sim 0.1$. We therefore use this shifted line to divide the two for the SDSS galaxy samples. The blue population, as shown in Figure 2, evolves more with redshift than the red-sequence galaxies, with the blue cloud being roughly 0.2–0.3 magnitudes redder

at $z \sim 0$ relative to $z \sim 1$. Previous analysis by Blanton (2006) found this evolution in color between the SDSS and DEEP2 to be consistent with the global decline in the star-formation rate. For a more complete discussion of the evolution in the color-magnitude distribution of galaxies in SDSS and DEEP2, we direct the reader to Blanton (2006).

2.2. Sample Selection

As with most deep redshift surveys, the DEEP2 spectroscopic targets span a broad range in redshift, but were selected according to a fixed apparent-magnitude limit. The DEEP2 $R_{AB} = 24.1$ magnitude limit includes different portions of the galaxy population (in rest-frame color-magnitude space) at different redshifts. To allow

tests of how this selection effect could influence our results, we employ a variety of subsamples from the full catalog of 15,987 DEEP2 galaxies in the redshift range $0.75 < z < 1.05$ (which we define to be Sample DEEP2-A).

As discussed by Gerke et al. (2007) and Cooper et al. (2007), it is possible to produce volume-limited catalogs with a color-dependent absolute-magnitude cut by defining a region of rest-frame color-magnitude space that is included by the survey at all redshifts of interest. For the DEEP2 survey, such a selection cut is illustrated in the top panel of Figure 3 and given by

$$M_{\text{cut}}(z, U - B) = Q(z - z_{\text{lim}}) + \min \{ [a(U - B) + b], [c(U - B) + d] \}, \quad (2)$$

where z_{lim} is the limiting redshift beyond which the selected sample becomes incomplete, a , b , c and d are constants that are determined by the limit of the color-magnitude distribution of the sample with redshift $z > z_{\text{lim}}$, and Q is a constant that allows for linear redshift evolution of the typical galaxy absolute magnitude, M_B^* . For this parameter, we adopt a value of $Q = -1.37$, determined by Faber et al. (2007) from a study of the B -band galaxy luminosity function in the COMBO-17 (Wolf et al. 2001), DEEP1 (Vogt et al. 2005), and DEEP2 (Davis et al. 2003) surveys. Varying our choice of Q by as much as $\sim 40\%$ has a negligible effect on our results.

By including this linear M_B^* evolution in our selection cut, we are selecting a similar population of galaxies with respect to M_B^* at all redshifts. Adopting this approach, with a limiting redshift of $z_{\text{lim}} = 1.05$, we define a sample of 12,198 galaxies (Sample DEEP2-B) over the redshift range $0.75 < z < 1.05$ that is volume-limited relative to M_B^* and selected according to a color-dependent cut in M_B . The values of the constants a , b , c , and d which define the color-dependent selection are -1.6 , -18.65 , -2.55 , and -17.7 , respectively. For complete details of the selection method, we refer the reader to Gerke et al. (2007).

A somewhat simpler selection method is to produce a subsample that is volume-limited relative to M_B^* according to a color-independent cut in absolute magnitude. We create such a sample (Sample DEEP2-C) by restricting to $0.75 < z < 1.05$ and requiring

$$M_B(z) \leq -20.6 + Q(z - z_{\text{lim}}), \quad (3)$$

where $M_B = -20.6$ is the absolute magnitude to which DEEP2 is complete along both the red sequence and the blue cloud at $z_{\text{lim}} = 1.05$ (cf. the top panel of Figure 3). A brief summary of all galaxy samples utilized in this paper is provided in Table 1.

To facilitate the comparison of trends with local environment at $z \sim 0.1$ to those at $z \sim 1$, we select subsamples drawn from the SDSS which mimic the DEEP2 survey subsamples detailed above. While both the SDSS and DEEP2 spectroscopic targets are selected according to an apparent-magnitude limit in a red optical band ($r \leq 17.77$ and $R \leq 24.1$, respectively), this band falls in a very different part of the spectrum in the rest-frame at the two redshift ranges probed. At $z \sim 0.1$ the center of the SDSS r passband corresponds to a rest-frame wavelength of 5605\AA , whereas at $z \sim 1$ the CFHT R

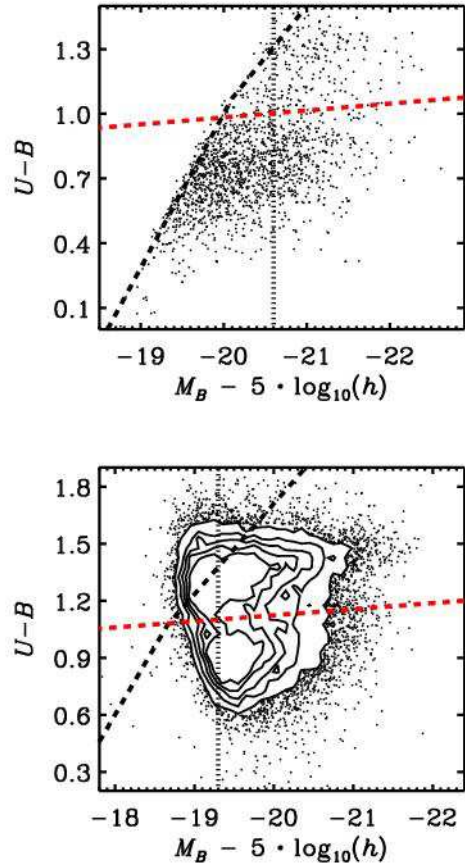


FIG. 3.— (Top) The rest-frame color-magnitude diagram for all DEEP2 galaxies in the redshift range $1.025 < z < 1.075$. The black dotted vertical line defines the color-independent completeness limit of the DEEP2 survey at $z = 1.05$, providing the absolute-magnitude limit used for Sample DEEP2-C. To this limit, DEEP2 is complete for galaxies of all colors at $z < 1.05$. The black dashed line defines the completeness limit of the DEEP2 survey as a function of rest-frame color at redshift $z = 1.05$ and corresponds to Equation 2. (Bottom) The rest-frame color-magnitude diagram for all SDSS galaxies in the redshift range $0.095 < z < 0.105$. The dotted and dashed black vertical lines follow the corresponding limits from the top panel, allowing for evolution in M_B^* as given in Equation 2 and Equation 3. The dashed red line in each plot indicates our division between the red sequence and the blue cloud, as given by Equation 1. Due to the large number of galaxies in the SDSS sample, we plot contours corresponding to 20, 40, 60, 80, and 100 galaxies per bin of $\Delta(U - B) = 0.05$ and $\Delta M_B = 0.1$.

passband employed by DEEP2 samples a portion of rest-frame wavelength space centered on roughly 3300\AA , well into the ultraviolet. As a result, the DEEP2 sample is biased towards blue (in rest-frame $U - B$ color) galaxies relative to the SDSS data set; in fact, DEEP2 probes to much fainter luminosities on the blue cloud (relative to L_B^*) than the SDSS sample, as shown in Figure 3. For this reason, we are unable to define an SDSS subsample that totally matches the DEEP2-B sample.

However, we can define two subsamples drawn from the full SDSS data set of 132,367 galaxies at $0.05 < z < 0.1$ (Sample SDSS-A) which complement the DEEP2-C sample. First, we select an SDSS subsample (Sample SDSS-B) that adheres to the same selection limit as the DEEP2-C galaxy sample. That is, we define an SDSS sample that is volume-limited relative to M_B^* , according

TABLE 1
DESCRIPTORS OF THE SDSS AND DEEP2 GALAXY SAMPLES

Sample	N_{galaxies}	$N_{\text{edge-cut}}$	N_{SFR}	z range	Brief Description
DEEP2-A	15,987	12,240	11,875	$0.75 < z < 1.05$	all galaxies after boundary cut
DEEP2-B	12,198	9,346	9,067	$0.75 < z < 1.05$	color-dependent limit, with limit held constant relative to $M_B^*(z)$
DEEP2-C	4,387	3,349	3,178	$0.75 < z < 1.05$	color-independent limit, with limit held constant relative to $M_B^*(z)$ and set as $M_B = -20.6$ at $z = 1.05$
SDSS-A	132,367	122,577	120,636	$0.05 < z < 0.1$	all galaxies after boundary cut
SDSS-B	61,413	57,051	56,118	$0.05 < z < 0.1$	color-independent limit, with limit held constant relative to $M_B^*(z)$ and set as $M_B = -20.6$ at $z = 1.05$
SDSS-C	42,991	39,978	39,254	$0.05 < z < 0.1$	color-independent limit, with limit held constant relative to $M_B^*(z)$ and set as $M_B = -20.6$ at $z = 1.05$; matched to DEEP2 red fraction

NOTE. — We list each galaxy sample employed in the analysis, detailing the selection cut used to define the sample as well as the redshift range covered and the number of galaxies included before (N_{galaxies}) and after ($N_{\text{edge-cut}}$) removing those within $1 h^{-1}$ comoving Mpc of a survey edge. The number of galaxies with an accurate SFR measurement and away from a survey edge is given by N_{SFR} .

to the color-independent cut in absolute magnitude given in Equation 3.

Within both the SDSS and DEEP2 galaxy catalogs, the bimodality of galaxy colors in rest-frame $U-B$ color is clearly visible (cf. Fig. 2 and Fig. 3). To quantify the composition of the SDSS and DEEP2 data sets in terms of red and blue galaxies, we compute the fraction of galaxies on the red sequence in each survey sample using the color divisions defined above (cf. Equation 1, offset by 0.14 magnitudes for the SDSS as described in §2.1).

Studies of the galaxy luminosity function at $z < 1$ have shown that the number density of galaxies on the red sequence has increased over the last 7 Gyr, yielding an increase in the red galaxy luminosity density of \gtrsim a factor of 2 (Bell et al. 2004; Faber et al. 2007). Meanwhile, the luminosity and number density of galaxies on the blue cloud has remained roughly constant (especially relative to that of the red sequence) over the same timespan.⁸ Thus, the relative fractions of red and blue galaxies in magnitude-limited samples will vary with redshift. Using the divisions between red and blue galaxies defined above, the fraction of galaxies which are on the red sequence in samples DEEP2-C and SDSS-B is 0.39 and 0.56, respectively. Because red-sequence galaxies are forming few stars, we might expect the overall average SFR in galaxies in the SDSS to be lower simply due to this greater fraction of quiescent galaxies, rather than through a modulation of the rate in star-forming objects.

To select a sample from the SDSS that is more analogous to the DEEP2-C sample (i.e., yielding an equivalent red fraction down to the common magnitude limit), we randomly throw out red galaxies from SDSS-B. The resulting sample (SDSS-C) contains 42,991 galaxies with

a distribution of rest-frame colors comparable to that of DEEP2-B, as shown in Figure 4, and a red fraction of 0.39. We have not required the SDSS galaxies to follow the same absolute-magnitude distribution as the DEEP2-C sample. However, the dependence of the fraction of red (or blue) galaxies on $M_B - M_B^*$ in the SDSS-C and DEEP2-C samples are very similar (as shown in Figure 5), with blue galaxies dominating at faint luminosities and with blue and red populations each comprising roughly half of the population at the bright end of the M_B distribution. A summary of both the DEEP2 and SDSS galaxy samples is provided in Table 1.

2.3. Measurements of Local Galaxy Environment

For the purposes of this paper, we consider the “environment” of a galaxy to be defined by the local mass overdensity, measured using the local overdensity of galaxies as a proxy; over quasi-linear regimes, these should differ by a factor of the galaxy bias (Kaiser 1987). We estimate this overdensity for both the SDSS and DEEP2 using measurements of the projected 3rd-nearest-neighbor surface density (Σ_3) about each galaxy, where the surface density depends on the projected distance to the 3rd-nearest neighbor, $D_{p,3}$, as $\Sigma_3 = 3/(\pi D_{p,3}^2)$. In computing Σ_3 , a velocity window of ± 1000 km/s is employed to exclude foreground and background galaxies along the line-of-sight. Tests by Cooper et al. (2005) found this environment estimator to be a robust indicator of local galaxy density for the DEEP2 survey.

To correct for the redshift dependence of the sampling rate of both the SDSS and the DEEP2 surveys, each surface density value is divided by the median Σ_3 of galaxies at that redshift within a window of $\Delta z = 0.02$ and $\Delta z = 0.04$ for the SDSS and DEEP2, respectively; this converts the Σ_3 values into measures of overdensity relative to the median density (given by the notation $1 + \delta_3$ here) and effectively accounts for redshift variations in the selection rate (Cooper et al. 2005). In computing the local environment for galaxies in our targeted redshift ranges ($0.05 < z < 0.1$ for the SDSS and $0.75 < z < 1.05$ for DEEP2), we included sources at lower and higher

⁸ There is some debate within the community regarding the evolution in the number density of blue galaxies at intermediate and low redshift. Parallel studies of the luminosity and stellar mass functions at $z < 1$ have found significant evolution in the number density of bright (massive), blue galaxies (e.g., Bundy et al. 2006; Zucca et al. 2006).

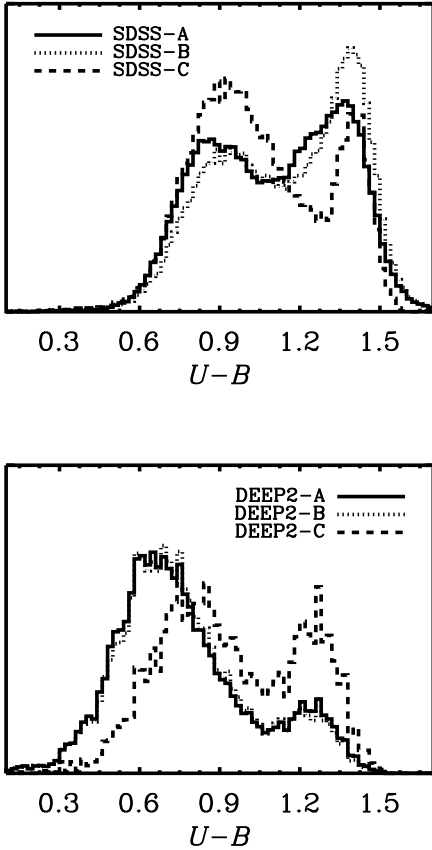


FIG. 4.— The relative distribution of rest-frame $U-B$ colors for the galaxy subsamples listed in Table 1. By randomly excluding red galaxies from the SDSS sample, we are able to define a subsample (SDSS-C) with a red-galaxy fraction comparable to that of the DEEP2-C sample. The plotted histograms have been normalized to have equal area.

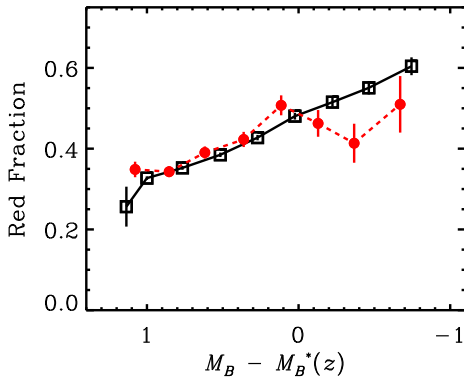


FIG. 5.— The fraction of red galaxies as a function of B -band absolute magnitude [relative to $M_B^*(z)$] for the SDSS-C (open black squares) and DEEP2-C (filled red circles) samples (i.e., the galaxy samples constructed to have color-independent M_B cuts and equivalent aggregate red-galaxy fractions). The red galaxy population is selected in each survey sample using the color divisions defined by Equation 1, offset by 0.14 magnitudes for the SDSS, with the error in the red fraction given by binomial statistics. We assume an evolution of 1.37 magnitudes per unit redshift ($Q = -1.37$) in $M_B^*(z)$, with $M_B^*(z = 0.9) = -21.48$ from Willmer et al. (2006).

redshifts as tracers of the galaxy distribution to avoid edge effects due to redshift limits; similarly, the smoothing windows for calculations of median Σ_3 include tracers outside the sample z limits.

Finally, to minimize the effects of edges and holes in the SDSS and DEEP2 survey geometries, we exclude all galaxies from our SDSS and DEEP2 samples within $1 h^{-1}$ Mpc (comoving) of a survey boundary, reducing our sample sizes to the numbers given in Table 1. In Figure 6, we plot the distribution of overdensities for the SDSS-A and DEEP2-A samples, after these edge cuts. For complete details regarding the computation of the local environment measures, we direct the reader to Cooper et al. (2006).

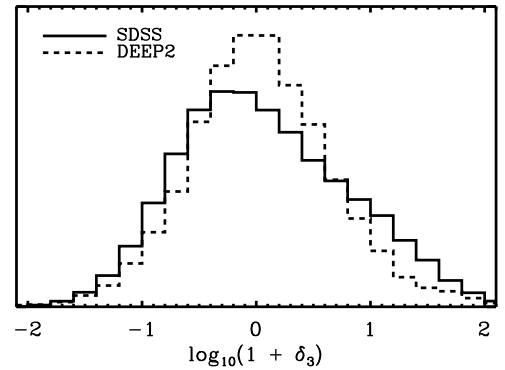


FIG. 6.— The distribution of the logarithm of the local overdensities, $\log_{10}(1 + \delta_3)$, for the DEEP2 and SDSS samples. We plot the environment distributions for the 12,240 DEEP2 galaxies with $0.75 < z < 1.05$ and more than $1 h^{-1}$ comoving Mpc from a survey edge (solid line) along with that for the 132,367 SDSS galaxies with $0.05 < z < 0.1$ and more than $1 h^{-1}$ comoving Mpc from a survey edge (dashed line). The overdensity, $(1 + \delta_3)$, is a dimensionless quantity, computed as described in §2.3. Here, we scale the DEEP2 and SDSS histograms so that their integrals are equal.

The overdensity distributions for the SDSS and DEEP2, as shown in Fig. 6, differ for several reasons. The first is simply the nonlinear growth of large-scale structure over time: a dense region on nonlinear scales will be denser at $z \sim 0$ than at $z \sim 1$, while a void will be less dense today than in the past. A second reason is that the average bias of the overall SDSS sample used as a tracer of density is higher than the overall DEEP2 sample (Zehavi et al. 2002, 2005; Coil et al. 2004b, 2006); this will cause density contrasts measured with galaxies to be exaggerated in the SDSS compared to DEEP2.

A third cause for the differences in these distributions is that we are using the projected 3rd-nearest-neighbor distance, $D_{p,3}$ to measure overdensity in both samples; but because the number density of the SDSS sample used to trace environment is higher than in DEEP2, the typical $D_{p,3}$ for the SDSS is smaller ($\sim 1 h^{-1}$ comoving Mpc) than for a DEEP2 galaxy ($\sim 1.8 h^{-1}$ comoving Mpc). Hence, in the SDSS, we are measuring overdensities on somewhat smaller, more highly nonlinear scales. However, Blanton et al. (2006) found that in the SDSS, environments measured on scales from 0.2 to 6 h^{-1} Mpc yield equivalent results; we therefore do not expect this to be a major issue.

All of these effects operate in the same sense, exag-

generating the density contrasts measured in the SDSS. However, none of them should change the rank ordering of overdensities. In this paper, we focus on changes in the general relationships between environment and galaxy properties (namely, star-formation activity) between $z \sim 0$ and $z \sim 1$; this requires only that we have an accurate measure of relative environment at each redshift. The $(1 + \delta_3)$ values provide such a tracer of local galaxy density at both epochs.

2.4. Measurements of Star-Formation Rates

We estimate the global star-formation rates for galaxies in both the SDSS and DEEP2 samples using measured [O II] $\lambda 3727\text{\AA}$ nebular line luminosities, corrected using the empirical calibration of Moustakas et al. (2006). Although this calibration was developed by tuning [O II]-derived star-formation rates (for dust extinction and metallicity) to match those based on extinction-corrected $H\alpha$ and far-infrared emission using multiwavelength observations of nearby galaxies, the results have been tested and proven effective at intermediate redshifts ($0.7 < z < 1.4$) (Moustakas et al. 2006). As will be shown in §5.3, however, the results presented in this paper are not sensitive to the particular calibration employed. Using star-formation rates derived with $1/2\times$ or $2\times$ the luminosity-dependence given by Moustakas et al. (2006), accounting for a wide range in possible dust and metallicity effects, using the calibrations of Kennicutt (1998) and Weiner et al. (2007), or using the SFR estimates of Tremonti et al. (2004), we find that our results regarding the relationships between star formation, color, and environment at $z \sim 0.1$ and $z \sim 1$ remain unchanged. For both the SDSS and DEEP2 galaxy samples, all estimated star-formation rates are given in units of $h^{-2}M_{\odot}\text{yr}^{-2}$. As noted in Table 1, a small number of objects in both the SDSS and DEEP2 were rejected from the galaxy samples due to large uncertainties in their measured [O II] line fluxes ($\sigma_{[\text{OII}]} > 500 \times 10^{-19} \text{ ergs}^{-1}\text{cm}^2$).

For the DEEP2 sample, we measure [O II] equivalent widths using a nonlinear least-squares fit to the observed emission lines in the DEEP2/DEIMOS spectra, using a model given by two Gaussians of the same width (σ), centered at the known rest-frame wavelengths of the two components of the doublet. The continuum level is estimated from the biweight of the continuum in two windows, $15\text{--}60\text{\AA}$ away from the emission line in the rest-frame. The observed $R - I$ color and I magnitude for each galaxy is used to estimate its continuum luminosity at 3727\AA via the K-correction procedure of Willmer et al. (2006). Combined with the measured [O II] equivalent width, this yields a flux-calibrated line luminosity. The line luminosities are then transformed into star-formation rates using a correction factor based upon the galaxy's B -band absolute magnitude, as given by a linear interpolation of the values in Table 2 of Moustakas et al. (2006); we test the impact of using other conversions in §5.3. For complete details regarding the computation of [O II] emission-line luminosities in DEEP2, see Weiner et al. (2007).

We estimate the [O II] luminosities for SDSS galaxies by measuring the total observed line flux in the spectrum. This gives the [O II] luminosity integrated over the area

covered by the SDSS fiber, which might be an underestimate of a galaxy's true total [O II] luminosity, given the limited angular size of the SDSS fibers. Alternatively, we can estimate the true total [O II] luminosity by combining a measurement of the [O II] equivalent width with the K-corrected u -band absolute magnitude (i.e., assuming that the ratio of [O II] flux to u flux is uniform across the entire galaxy). This yields a significantly less precise measure of the [O II] luminosity, due to the high noise level in SDSS u -band photometry. Nevertheless, if we were to adopt these noisier SFR estimates, none of our conclusions would be changed.

We measure the [O II] line flux for SDSS galaxies in a 22\AA window around the line after removing all stellar continuum features from the spectra. The stellar continua around 3727\AA are very bumpy and would introduce systematic [O II] flux offsets if not accurately subtracted. The subtraction procedure used is described in Yan et al. (2006); we summarize here. After subtracting off the continuum of the spectrum smoothed over a broad window, the stellar continuum is fit to a linear combination of two stellar population templates produced with Bruzual & Charlot models (Bruzual & Charlot 2003), again with their broad continuum components subtracted. One template is the spectrum of a 7-Gyr-old simple stellar population, while the other corresponds to a 0.3-Gyr-old starburst of duration 0.1 Gyr (i.e., a starburst commencing 0.4 Gyr in the past). This combination of templates, each constructed with solar metallicity, has proven adequate to accurately describe the wiggles in the continuum near [O II] for most galaxies in the SDSS. With the stellar continuum features removed, we measure the line flux in the remaining, emission-line only spectrum. The uncertainties in this continuum subtraction have been propagated into our error estimates for [O II] fluxes.

2.5. Measurements of Stellar Masses

Stellar masses for the SDSS galaxies were determined using the *kcorrect* K-correction code of Blanton et al. (2003). The template SEDs employed by *kcorrect* are based on those of Bruzual & Charlot (2003); the best-fit SED given the observed *ugriz* photometry and spectroscopic redshift can be used directly to estimate the stellar mass-to-light ratio (M_*/L), assuming a Chabrier (2003) initial mass function.

For a portion of the DEEP2 galaxy catalog, stellar masses may be calculated using WIRC/Palomar J - and K_s -band photometry in conjunction with the DEEP2 *BRIJK_s* data (Bundy et al. 2006). The observed (*BRIJK_s*) SED of each K_s -detected galaxy is compared to a grid of 13440 synthetic SEDs from Bruzual & Charlot (2003), which span a range of star-formation histories, ages, metallicities, and dust content, and use a Chabrier (2003) initial mass function (Bundy et al. 2005). From fits to the grid of models, a stellar-mass probability distribution is obtained after scaling each model's M_*/L_K ratio to the total K_s magnitude and marginalizing over the grid. The median of this distribution is taken as the stellar mass estimate (Bundy et al. 2006).

The K_s -band photometry, however, does not cover the entire area of the DEEP2 survey, and often faint blue galaxies at the high- z end of the DEEP2 redshift range are not detected in K_s . Because of these two effects,

the stellar masses of Bundy et al. (2006) have been used to calibrate stellar mass estimates for the full DEEP2 sample that are based on combining rest-frame M_B and $B-V$ derived from the DEEP2 data (Lin et al. 2007) into the expressions of Bell et al. (2003), which use a “diet Salpeter” IMF and are valid at $z = 0$. We empirically correct these stellar mass estimates to the Bundy et al. (2006) measurements by accounting for a mild color and redshift dependence (Lin et al. 2007); where they overlap, the two stellar masses have an RMS difference of approximately 0.3 dex after this recalibration.

We note that while rest-frame B -band emission is more sensitive to the presence of young stars than redder bands, there is still a strong correlation between stellar mass and absolute B -band magnitude in both the SDSS and DEEP2 samples. As shown in Figure 7 and Figure 8, the RMS difference between M_* and M_B is roughly 0.5 dex; these differences are strongly correlated with rest-frame galaxy color.

By combining the measurements of total SFR and stellar mass estimates described above, we can compute the specific star-formation rate (sSFR) for each galaxy in the SDSS and DEEP2 samples. The sSFR describes the fractional rate of stellar mass growth ($\text{sSFR} = \text{SFR}/M_*$) in a galaxy due to ongoing star formation. The sSFR has units of inverse time; for this reason, galaxies with low specific star-formation rates are said to have long star-formation timescales and vice versa.

3. RESULTS

Because it is expected that the local environment of a galaxy should influence its properties (such as star-formation rate), it is common to study those properties as a function of environment. Since our tracers of environment are generally sparse, however, measurements of galaxy densities are generally significantly more uncertain than measures of most other properties such as color, luminosity, or even SFR. Therefore, binning galaxies according to local overdensity introduces a significant correlation between neighboring environment bins, which can smear out any underlying trends. In this paper, we study both the dependence of mean environment on galaxy properties and vice versa: the former minimizes covariance, while the latter eases comparison to other studies. Throughout §3, we show results for the SDSS-A and DEEP2-A samples, which probe the greatest range in luminosity and have the largest sample sizes. However, the qualitative relationships between environment and star formation for each of the galaxy subsamples in Table 1 are consistent with each other, with the normalization and strength of the trends varying amongst them (cf. Table 2 and Table 3). We present our principal results in this section; these results will be interpreted in §4 and the remainder of the paper.

3.1. The sSFR–density relation at $z \sim 0.1$ and $z \sim 1$

The connection between specific star-formation rate and environment at $z \sim 0$ has been explored by a number of previous studies utilizing samples drawn from the SDSS or other catalogs of nearby galaxies (e.g., Lewis et al. 2002; Gómez et al. 2003; Kauffmann et al. 2004). In agreement with these earlier analyses, we find that galaxies with lower specific star-formation rates, on

TABLE 2
FITS TO sSFR–DENSITY RELATION

Sample	a_0	a_1	σ_{a_0}	σ_{a_1}
DEEP2-A	-8.84	-0.060	0.013	0.020
DEEP2-B	-8.81	-0.067	0.011	0.017
DEEP2-C	-9.05	-0.067	0.007	0.011
SDSS-A	-10.24	-0.128	0.024	0.036
SDSS-B	-10.31	-0.124	0.023	0.033
SDSS-C	-10.19	-0.087	0.024	0.035

NOTE. — We list the coefficients and 1σ uncertainties for the parameters of the linear-regression fits to the sSFR–density relation given by $\log_{10}(< \text{sSFR} >) = a_1 * \log_{10}(1 + \delta_3) + a_0$ (cf. Fig. 10), for all galaxy samples used. For details regarding the various galaxy samples, refer to §2.2 and Table 1.

average, favor regions of higher galaxy density at $z \sim 0.1$ (cf. Figure 9a).

Using the DEEP2 data set to study galaxy properties at $z \sim 1$, we find that the dependence of mean environment on sSFR, as found in the SDSS-A sample, is echoed in the DEEP2-A sample. As shown in Figure 9, galaxies with longer star-formation timescales (i.e., lower specific star-formation rates) favor regions of higher galaxy density at both $z \sim 0.1$ and $z \sim 1$.

The same general trend is found when we examine the connection between sSFR and environment from the opposite perspective. Figure 10 shows the dependence of the mean galaxy sSFR on local overdensity in the SDSS-A and DEEP2-A samples. We find that, at $z \sim 0.1$ and at $z \sim 1$, galaxies residing in regions of higher density generally have lower specific star-formation rates. Moving to higher-density environments at $z \sim 0.1$ and at $z \sim 1$, the average specific star-formation rate declines monotonically such that members of clusters and massive groups, as a population, exhibit the longest star-formation timescales (or the lowest fractional rate of stellar mass growth).

All of the SDSS and DEEP2 samples described in §2.2 exhibit a highly significant anticorrelation between specific star-formation rate and galaxy environment. Table 2 lists the coefficients from linear-regression fits to the dependence of mean sSFR on overdensity in each galaxy sample. The fits to the SDSS-A and DEEP2-A samples are shown in Figure 10 as the dashed red lines. The slopes of the trends between mean sSFR and overdensity for each of the SDSS and DEEP2 subsamples agree within the uncertainties. Variations in normalization between subsamples are associated with differences in sample selection and galaxy evolution at $z < 1$; these effects are examined in more detail in §6.

3.2. The SFR–density relation at $z \sim 0.1$ and $z \sim 1$

As shown in Figure 11a, we find that for SDSS-A, the mean SFR of galaxies in the sample decreases in regions of higher overdensity, mimicking the sSFR–density relation observed both at $z \sim 0.1$ and at $z \sim 1$. In stark contrast, the mean SFR *increases* with local galaxy density at $z \sim 1$, an inversion of the local relation (cf. Fig. 11b). For each of the SDSS and DEEP2 samples, we find similar results to those shown in Figure 11. Table 3 provides the coefficients from linear-regression fits to the dependence of mean SFR on galaxy overdensity in

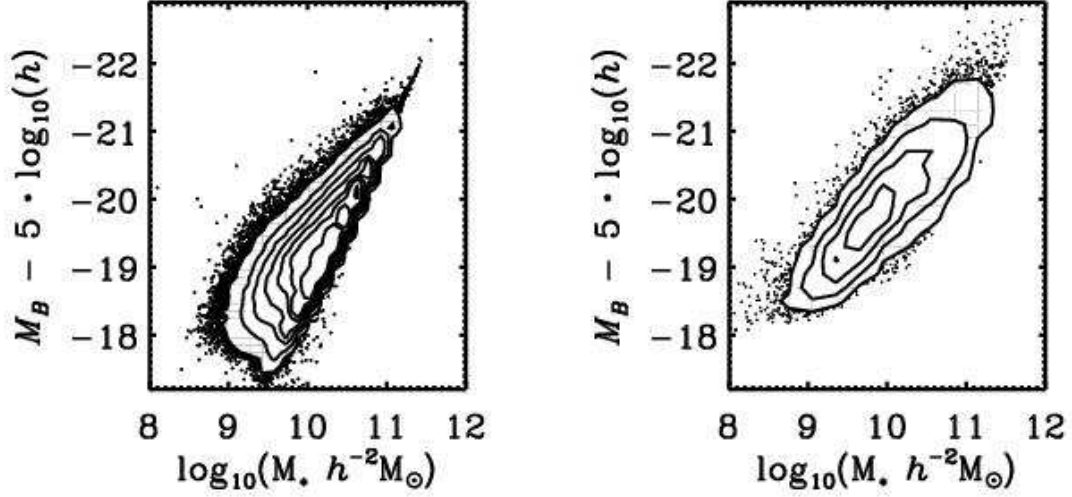


FIG. 7.— The relationship between stellar mass and absolute B -band magnitude for galaxies in the SDSS-A (*left*) and DEEP2-A (*right*) samples. There is a strong correlation between M_B and M_* in both galaxy samples. The contours correspond to 50, 150, 300, 500, 750, 1000, and 1500 galaxies per bin of $\Delta(\log_{10} M_*) = 0.15$ and $\Delta M_B = 0.1$ (*left*) and 50, 150, 300, 500, and 1000 galaxies per bin of $\Delta(\log_{10} M_*) = 0.3$ and $\Delta M_B = 0.2$ (*right*).

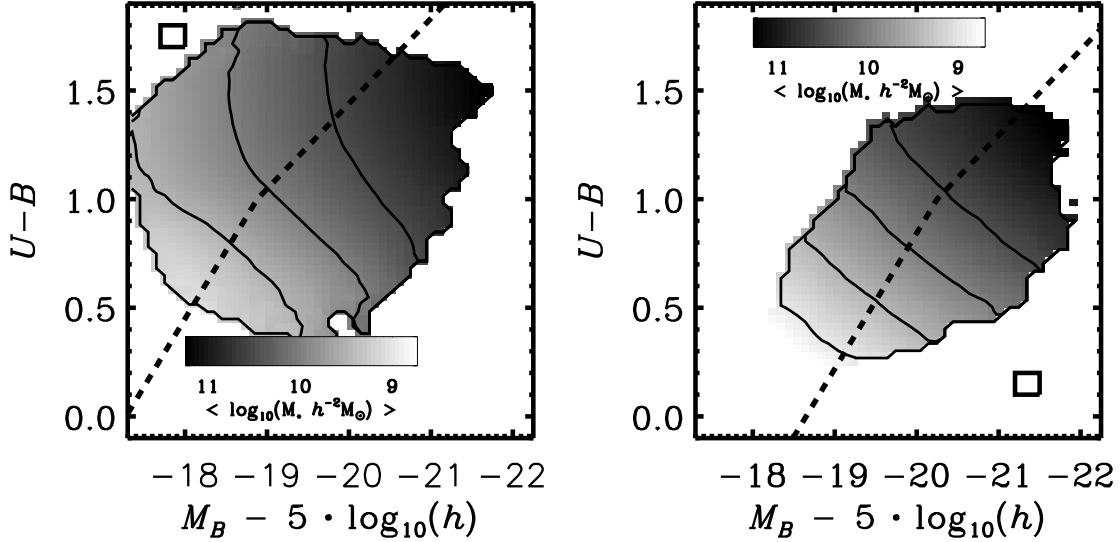


FIG. 8.— The mean stellar mass as a function of galaxy color, $U - B$, and absolute magnitude, M_B , for galaxies in the SDSS-A (*left*) and DEEP2-A (*right*) samples. The means are computed in a sliding box, illustrated in the corner of each plot, with width $\Delta M_B = 0.2$ and height $\Delta(U - B) = 0.1$. Darker areas in the image correspond to regions of higher average stellar mass in color–magnitude space with the scale given by the corresponding inset color bar. The contours in both plots correspond to levels of $\langle \log_{10}(M_*) \rangle = 9, 9.5, 10$, and 10.5 . At regions where the sliding box includes fewer than 20 galaxies, the mean stellar mass is not displayed. The dashed lines in each plot show the color–dependent, absolute–magnitude selection cut (cf. Equation 2) used in defining sample DEEP2-B.

each subsample described in §2.2. The fits to the SDSS-A and DEEP2-A samples are illustrated in Fig. 11 as dashed red lines. While the DEEP2-C sample yields no detectable correlation between mean SFR and environment, within the DEEP2-C sample we would have detected the same trend as seen in the SDSS-C sample at a $\sim 10\sigma$ level, given measurement errors.

Examining the dependence of mean environment on SFR, we find additional evidence that the relationship between star-formation activity and local environment at $z \sim 1$ was dissimilar from that observed at $z \sim$

0.1. In the local Universe, the mean galaxy overdensity smoothly decreases for galaxy populations with higher star-formation rates, as shown in Figure 12a. At higher redshift, however, the dependence of mean overdensity on SFR is considerably more complicated (cf. Fig. 12b), and is not a simple remapping of Fig. 11b. While the mean SFR for galaxies at $z \sim 1$ monotonically increases with increasing overdensity, the dependence of mean environment on SFR at $z \sim 1$ is a more complex, non-monotonic relation. This striking difference in the relationship between galaxy properties and environment at $z \sim 1$ and

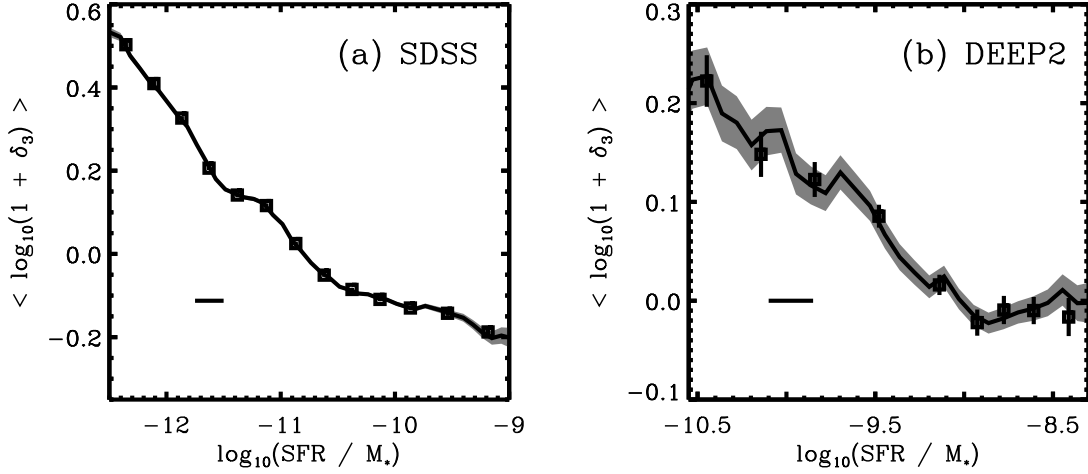


FIG. 9.— The relationship between mean environment and sSFR at $z \sim 0.1$ in the SDSS (*left*) and at $z \sim 1$ in DEEP2 (*right*). We plot the mean and the error in the mean of the logarithm of the local galaxy overdensity in discrete bins of sSFR (square points). The solid black lines show the mean dependence of environment on sSFR, where the means were computed using sliding boxes with widths given by the black dashes in the plot. The accompanying grey regions correspond to the sliding 1σ uncertainties in the means.

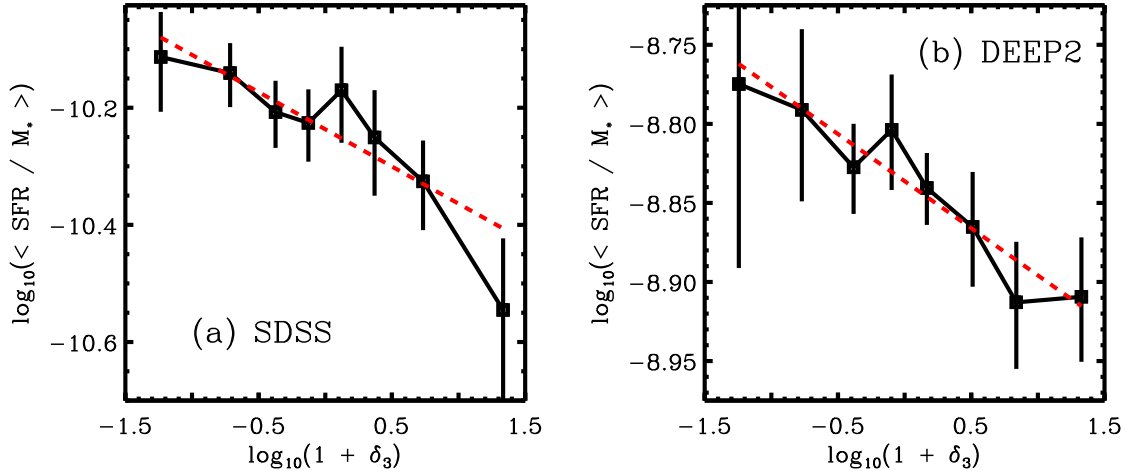


FIG. 10.— The dependence of mean sSFR on environment at $z \sim 0.1$ in the SDSS (*left*) and at $z \sim 1$ in DEEP2 (*right*). We plot the logarithm of the mean and of the error in the mean of the sSFR in discrete bins of galaxy overdensity within the SDSS-A and DEEP2-A samples. The dashed red line in each plot shows a least-squares linear-regression fit to the data points, with coefficients of the fits given in Table 2.

TABLE 3
FITS TO SFR-DENSITY RELATION

Sample	a_0	a_1	σ_{a_0}	σ_{a_1}
DEEP2-A	0.99	0.046	0.003	0.005
DEEP2-B	1.07	0.034	0.003	0.005
DEEP2-C	1.23	0.004	0.005	0.008
SDSS-A	-0.29	-0.108	0.004	0.005
SDSS-B	-0.16	-0.117	0.005	0.007
SDSS-C	-0.06	-0.082	0.005	0.008

NOTE. — We list the coefficients and 1σ uncertainties for the parameters of least-squares linear-regression fits to the SFR-density relation given by $\log_{10}(\langle \text{SFR} \rangle) = a_1 * \log_{10}(1 + \delta_3) + a_0$ (cf. Fig. 11), for all galaxy samples used. For details regarding the various galaxy samples, refer to §2.2 and Table 1.

at $z \sim 0.1$ requires explication.

4. INTERPRETING THE RESULTS

To have any hope of accurately characterizing the role of environment in the cosmic star-formation history, we must understand the differences between our results at $z \sim 1$ and the corresponding relations at $z \sim 0.1$. We begin by exploring the relationship between sSFR and environment, which shows qualitative agreement at low and intermediate redshifts.

4.1. Understanding the sSFR-density relation at $z < 1$

The sSFR-density relations at $z \sim 0.1$ and at $z \sim 1$ can be explained by the same fundamental physical phenomena that drive the color-density relation at $z < 1$. As first shown by Cooper et al. (2006), the general form of the color-density relation, as measured

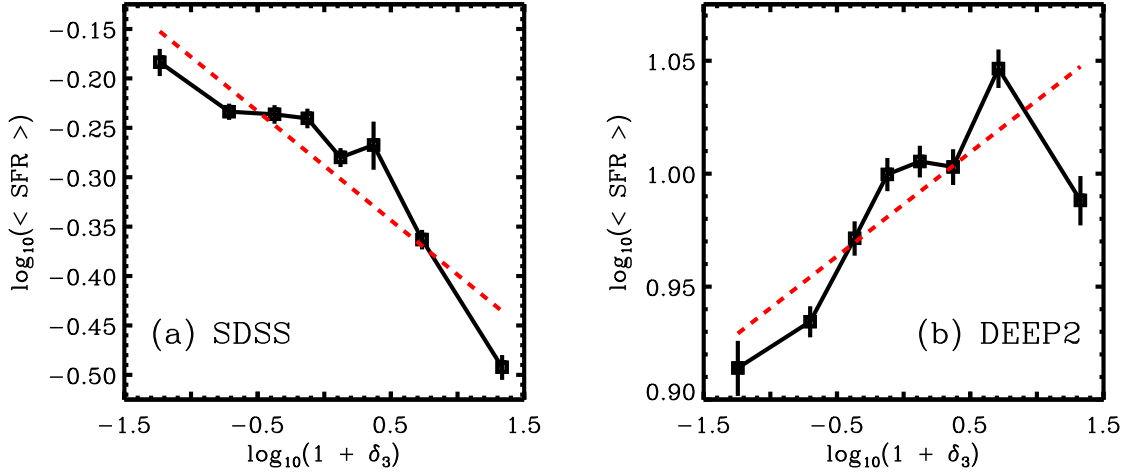


FIG. 11.— The dependence of mean SFR on environment at $z \sim 0.1$ (left) and at $z \sim 1$ (right). We plot the logarithm of the mean SFR and of the error in the mean SFR in discrete bins of galaxy overdensity within the SDSS-A and DEEP2-A samples. The dashed red line in each plot shows a linear-regression fit to the data points, with coefficients of the fits given in Table 3. Note that the star-formation rate (SFR) is given in units of $h^{-2} M_{\odot}/\text{yr}$.

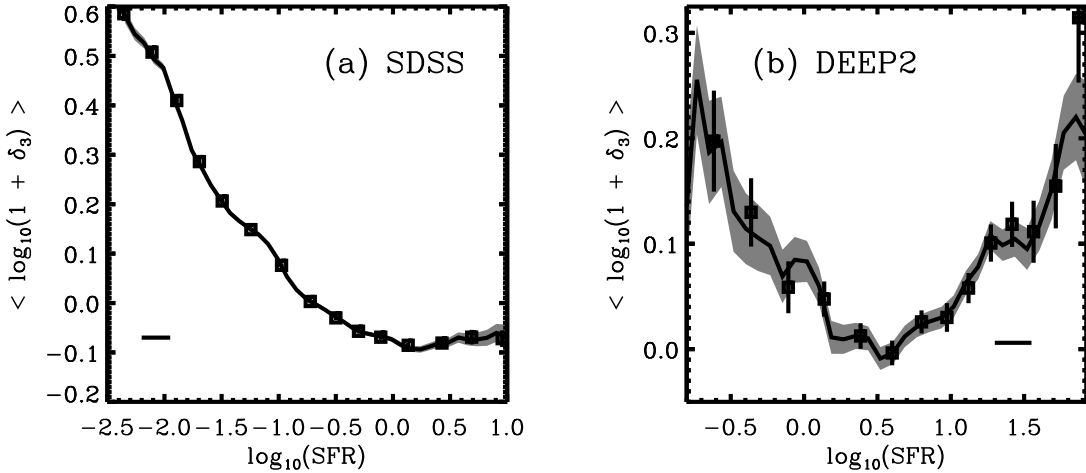


FIG. 12.— The dependence of the mean environment on SFR in the SDSS-A (left) and DEEP2-A (right) samples. We plot the mean and the error in the mean of the logarithm of the local galaxy overdensity in discrete bins of SFR (square points). The solid black lines show the mean dependence of environment on SFR, where the means were computed using sliding boxes with widths given by the black dashes in the plot. The accompanying grey regions correspond to the sliding 1σ uncertainties in the means. Note that the mean star-formation rate is given in units of $h^{-2} M_{\odot}/\text{yr}$.

locally (Blanton et al. 2005a), was already established when the Universe was half its present age, with red galaxies, on average, favoring regions of higher density relative to their blue counterparts. This strong effect, which is well studied at low and intermediate redshift (e.g., Hogg et al. 2003; Balogh et al. 2004b; Nuijten et al. 2005; Baldry et al. 2006; Weinmann et al. 2006), likely results from the quenching of star formation occurring more efficiently in regions of higher galaxy density. Many physical processes, from ram-pressure stripping to galaxy mergers, naturally produce such a connection between the star-formation history of a galaxy and its local environment (for a more complete discussion of likely mechanisms, see Cooper et al. 2006).

To illustrate the connection between the sSFR-density and color-density relations, it is essential to understand

the relationship between sSFR and rest-frame color at $z < 1$. The specific star-formation rate measures the marginal rate of ongoing star-formation activity in a galaxy. On the other hand, rest-frame $U - B$ color is a tracer of a galaxy's star-formation history on roughly Gyr timescales. Although galaxy color and sSFR measure star-formation activity on different timescales, Figure 13 shows that there is a close relationship between the two galaxy properties at $z \sim 0.1$ and particularly at $z \sim 1$ (where $U - B$ colors are better determined). All of the highest-sSFR galaxies are blue, while redder galaxies have longer star-formation timescales. Because of the differences in timescales probed by [O II] emission ($\lesssim 10^7$ years) and the color of stellar populations, the tightness of this relationship at $z \sim 1$ suggests that the DEEP2 sample is dominated by galaxies with a smoothly

evolving star-formation rate, rather than undergoing a series of brief, violent star-formation episodes (see also Noeske et al. 2007b).

The connection between sSFR and color is even more striking in Figure 14, where we present the mean sSFR as a function of $U - B$ color and absolute magnitude, M_B . Both locally and at intermediate redshift, the mean galaxy sSFR is nearly independent of luminosity at fixed color. Along the red sequence at $z \sim 0.1$, there is some dependence on absolute magnitude, such that sSFR is lower in brighter red galaxies. This magnitude dependence is partially responsible for the greater scatter in the correlation between sSFR and $U - B$ color in Fig. 13a (relative to Fig. 13b); the much larger uncertainties in SDSS $U - B$ colors, compared to DEEP2, is also important. Galaxies in the most massive clusters in the SDSS, which are too rare to be probed significantly by DEEP2 (Gerke et al. 2005), may also influence the gradient in mean sSFR along the red sequence at $z \sim 0.1$. A number of physical processes which are expected only to be significant in such extreme environments can strip gas from cluster members, thereby cutting off star formation. Furthermore, clusters are often home to the most massive red-sequence galaxies, which bias the luminous red galaxy population to low sSFR. Another source of scatter between specific star-formation rates derived from [O II] emission and rest-frame color along the red sequence is the higher rate of AGN/LINER activity among the red-sequence population. This point is discussed in more detail in §5.2.

The steepening of the relationship between mean environment and sSFR (cf. Fig. 9) at very low specific star-formation rates can also be understood in terms of the color-density relation. At $\log_{10}(\text{sSFR}) \lesssim -10.5 \text{ yr}^{-1}$ in the SDSS and $\log_{10}(\text{sSFR}) \lesssim -9 \text{ yr}^{-1}$ in DEEP2, the sSFR-density relation increases in strength such that the mean overdensity rises dramatically for galaxies with longer star-formation timescales. At these very low specific star-formation rates, the SDSS and DEEP2 samples transition from being dominated by blue galaxies to members of the red sequence (cf. Fig. 13). As shown in Figure 5 of Cooper et al. (2006) and Figure 2 of Blanton et al. (2005a), the average overdensity exhibits a similarly sharp rise at the transition from the blue cloud to the red sequence. This relatively strong change from a blue galaxy population with short star-formation timescales typically residing in environments near the mean cosmic density, to a red population with low specific star-formation rates commonly located in higher-density regions, indicates that local environment plays a central role in the truncation of star formation in galaxies at $z < 1$.

Considering previous studies of galaxy properties at $0 < z < 1$, the close connection between environment, color, and sSFR is not particularly surprising. From a study of [O II] equivalent width, which roughly traces sSFR, in clusters and field samples at slightly lower redshifts ($0.18 < z < 0.55$), Balogh et al. (1998) arrived at a similar result, finding that the typical [O II] equivalent width for a galaxy decreases as a function of clustercentric radius. Furthermore, using data from the DEEP2 survey to study galaxy environments at $z \sim 1$, Cooper et al. (2006) found that [O II] equivalent width

(which is closely correlated with sSFR) is anticorrelated with local galaxy density, on average.

4.2. Understanding the SFR-density relation at $z < 1$

As discussed above, the specific star-formation rates in nearby galaxies are closely tied to their rest-frame $U - B$ colors. For *total* SFR, however, the connection to rest-frame color is not nearly as simple. In Figure 15, we show the relationship between total SFR and galaxy color at $z \sim 0.1$ and at $z \sim 1$. At constant color, the range of star-formation rates can exceed two orders of magnitude.

Though there is an overall trend between SFR and $U - B$ color, the correlation is much weaker than that seen between sSFR and $U - B$ color (cf. Fig. 13). The factor of stellar mass which distinguishes sSFR from SFR is the logical culprit. When we examine the mean SFR as a function of both $U - B$ color and absolute magnitude, M_B , we find that, unlike the mean sSFR, the mean SFR is far from independent of M_B ; in Figure 16, the isocontours of mean SFR run diagonally.⁹ This is little surprise, since sSFR is closely related to galaxy color, as shown in Fig. 13, and (M_*/L) is to first order simply a function of color, as described in §2.5; so total SFR is, roughly, a product of two functions of color alone (sSFR and (M_*/L_B) with the luminosity defined by M_B). Thus, evolution in the relationship between global SFR and environment is closely tied to evolution in the relationships between $U - B$ and environment as well as M_B and environment, not just one or the other.

Using data from the DEEP2 survey, Cooper et al. (2006) explored the dependence of mean environment on the two dimensions of galaxy color and absolute magnitude at $z \sim 1$. One of the chief results from this work was the discovery that for galaxies in the blue cloud the mean galaxy environment depends on M_B . In contrast, previous studies at $z \sim 0$ found that mean galaxy overdensity is essentially independent of absolute magnitude for the blue galaxy population (e.g., Hogg et al. 2004; Blanton et al. 2005a). In Figure 17, we show the mean absolute B -band magnitude as a function of local overdensity for blue galaxies in the SDSS and DEEP2 survey; while the mean M_B among nearby galaxies varies only weakly as a function of $1 + \delta_3$, the same trend at $z \sim 1$ shows a significant gradient, such that the average absolute magnitude of galaxies in regions of higher galaxy density is brighter. From linear-regression fits to the data points in Fig. 17, we find that the slope of the relationship between mean absolute magnitude (M_B) and environment for blue galaxies is a factor of > 5 greater at $z \sim 1$ than that found locally.

This difference in the relationship between environment and absolute magnitude (and therefore stellar mass — cf. Fig. 8) within the blue galaxy populations at $z \sim 0.1$ and $z \sim 1$ is reflected in the observed inversion in the mean SFR-environment relationship. In combination with the color-density relation, it can explain the trends found in both Fig. 11 and Fig. 12. When plotting the mean SFR as a function of environment at $z \sim 1$, each bin in overdensity is dominated by galaxies residing in the blue cloud, given DEEP2's bias towards the

⁹ The difference in the slope of the isocontours of mean SFR in the SDSS and DEEP2 samples is discussed in more detail in §5.3.

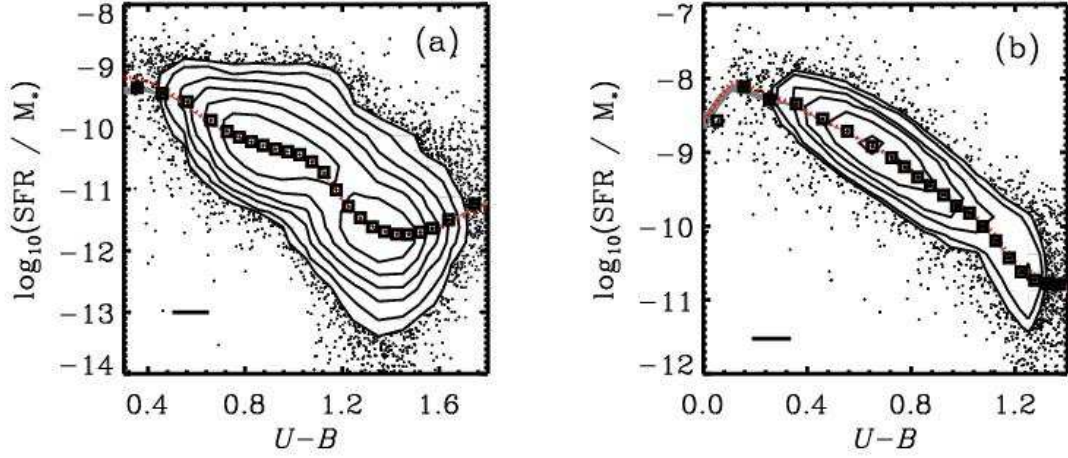


FIG. 13.— The relationship between $\log_{10}(\text{sSFR})$ and rest-frame color in the SDSS-A (*left*) and DEEP2-A (*right*) samples. We plot the mean *square points* and the error in the mean *grey region* of $\log_{10}(\text{sSFR})$ in bins of rest-frame $U-B$ color. The *red dotted lines* illustrate the median relation in the same sliding bins.

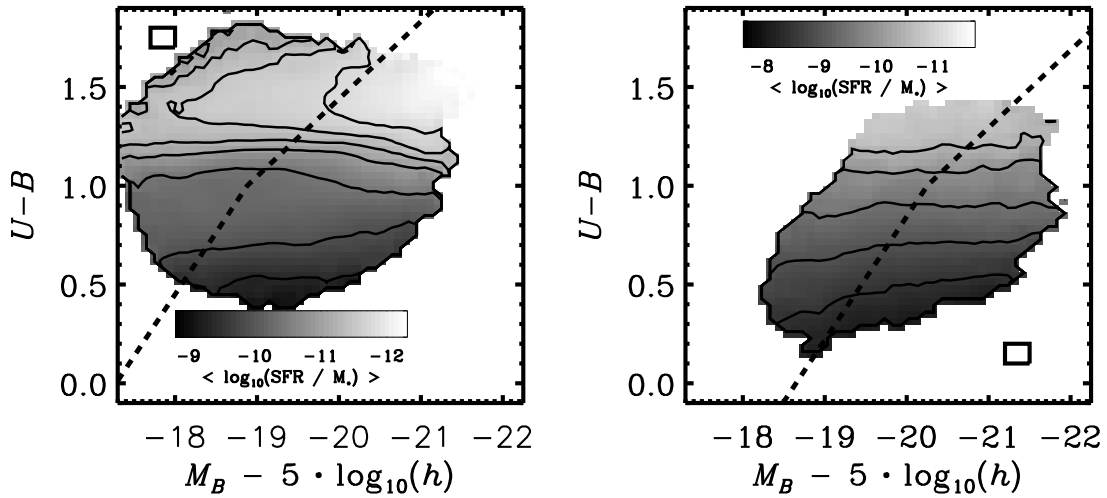


FIG. 14.— The mean sSFR as a function of galaxy color, $U-B$, and absolute magnitude, M_B , for galaxies in the SDSS-A (*left*) and DEEP2-A (*right*) samples. The means are computed in a sliding box, illustrated in the corner of each plot, with width $\Delta M_B = 0.3$ and height $\Delta(U-B) = 0.1$. Darker areas in the image correspond to regions of higher average sSFR in color-magnitude space with the scale given by the corresponding inset color bar. The contours in the respective plots correspond to levels of $\langle \log_{10}(\text{sSFR}) \rangle = -11.75, -11.5, -11.25, -11, -10.5, -10, -9.5$ (*left*) and $\langle \log_{10}(\text{sSFR}) \rangle = -10.5, -10, -9.5, -9, -8.5$ (*right*). At regions where the sliding box includes less than 20 galaxies, the mean sSFR is not displayed. The dashed lines in each plot show the color-dependent, absolute-magnitude selection cut (cf. Equation 2) used in defining sample DEEP2-B.

blue galaxy population. Thus, in Fig. 11b, we simply see an increase in mean SFR with overdensity, tracking the trend between mean M_B and environment for blue galaxies (cf. Fig. 17). At the highest galaxy densities, the contribution of red galaxies to the DEEP2 sample peaks and contributes to the flattening of this relationship.

In Fig. 12, on the other hand, we see a U-shaped trend when plotting mean environment as a function of SFR at $z \sim 1$. At the lowest SFRs, the sample is dominated by the red galaxy population (cf. Fig. 16), which are quenched entirely. Thus, we measure a high average overdensity for galaxies with low levels of star-formation activity, driven by the color-density relation; red galaxies typically favor regions of higher galaxy density, at both $z \sim 0.1$ and $z \sim 1$. At somewhat higher SFRs, the

sample becomes a mix of galaxies on the red sequence and fainter galaxies on the blue cloud, so the mean environment drops, reflecting the color-density relation. At $\log_{10}(\text{SFR}) \gtrsim 0.8 M_*/\text{yr}$, however, the mean overdensity begins to rise as the sample becomes entirely composed of increasingly brighter blue, star-forming galaxies. At these high SFRs, we therefore find the same relation as seen in Fig. 11b, where the mean overdensity increases with SFR.

5. POTENTIAL SYSTEMATIC EFFECTS

5.1. Isolating the Blue Cloud

As briefly discussed in §2, the galaxy population at $z \lesssim 1$ is bimodal in nature, with galaxies both locally and out to intermediate redshifts divisible into two dis-

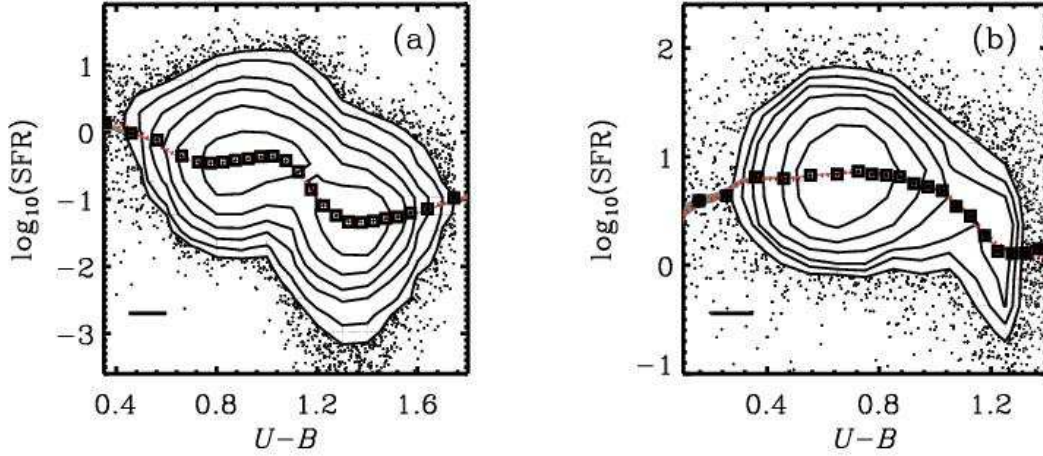


FIG. 15.— The relationship between $\log_{10}(\text{SFR})$ and rest-frame color in the SDSS-A (*left*) and DEEP2-A (*right*) samples. We plot the mean *square points* and the error in the mean *grey region* of $\log_{10}(\text{SFR})$ in bins of rest-frame $U - B$ color. The *red dotted lines* illustrate the median relation in the same sliding bins.

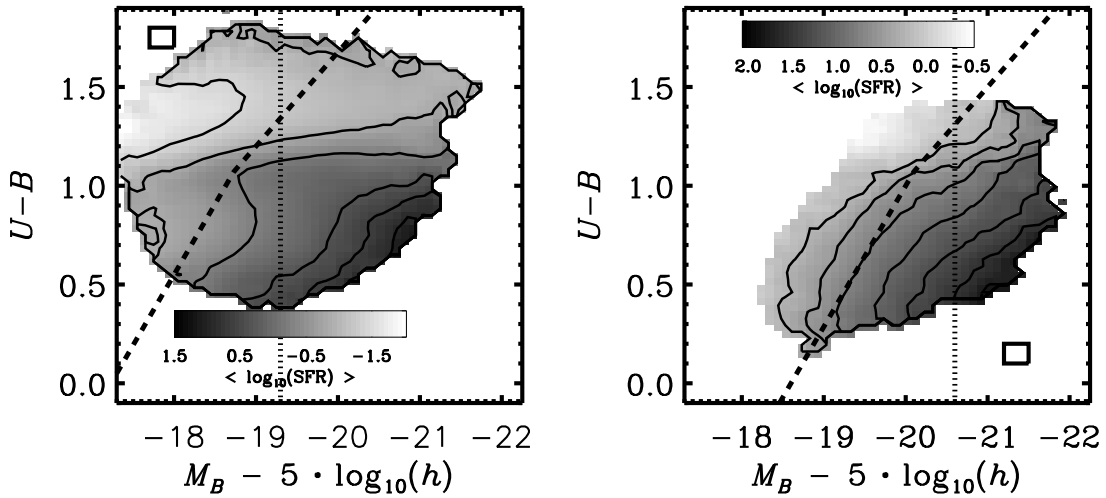


FIG. 16.— The mean SFR as a function of galaxy color, $U - B$, and absolute magnitude, M_B , for galaxies in the SDSS-A (*left*) and DEEP2-A (*right*) samples. The means are computed in a sliding box, illustrated in the corner of each plot, with width $\Delta M_B = 0.3$ and height $\Delta(U - B) = 0.1$. Darker areas in the image correspond to regions of higher average star-formation activity in color-magnitude space with the scale given by the corresponding inset color bar. The contours in the respective plots correspond to levels of $\langle \log_{10}(\text{SFR}) \rangle \geq -1.5, -1, -0.5, 0.0, 0.25, 0.5$ (*left*), and $\langle \log_{10}(\text{SFR}) \rangle \geq 0.25, 0.5, 0.75, 1, 1.25, 1.5, 1.75$ (*right*). At regions where the sliding box includes less than 20 galaxies, the mean SFR is not displayed. The dashed lines in each plot show the color-dependent, absolute-magnitude selection cut (cf. Equation 2) used in defining sample DEEP2-B.

tinct types: red, early-type galaxies lacking much star formation and blue, late-type galaxies with active star formation. Separating these two galaxy populations as described in §2.1, we can study the blue (“star-forming”) population in isolation while eliminating any relative bias towards one or the other type of galaxy in the SDSS and DEEP2 samples. The SDSS-C sample, which has a red fraction matched to that of the DEEP2-C sample, also provides a test for such selection effects. Additionally, this can facilitate comparison to other environment studies which only include star-forming galaxies (e.g., Elbaz et al. 2007).

We find that the trends of sSFR and SFR with environment discussed in §3 at $z \sim 0$ and $z \sim 1$ persist if we restrict samples to only the blue, star-forming population.

Table 4 lists the coefficients from linear-regression fits to the dependence of mean SFR (and sSFR) on overdensity in the SDSS-A and DEEP2-A galaxy samples, isolating simply the blue-cloud population. For both the SDSS and DEEP2 samples, the dependence of mean sSFR on local overdensity is weaker when excluding the red sequence. As discussed in §4, the sSFR-density relation is effectively tracing the color-density relation, which is dominated by the tendency of red galaxies – which have been removed here – to be found in dense regions.

When measuring the dependence of mean SFR on local galaxy density, we find that the relation is weaker in the SDSS blue-cloud population than in the full SDSS-A sample. However, we still detect a significant trend, with the mean SFR of the star-forming population be-

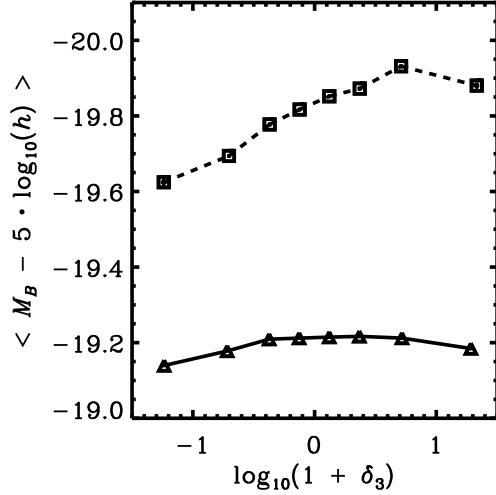


FIG. 17.— The mean absolute B -band magnitude, M_B for blue galaxies in the SDSS-A (solid line and triangles) and DEEP2-A (dashed line and squares) samples, in bins of local galaxy overdensity, $1 + \delta_3$. The blue galaxy populations within the SDSS and DEEP2 samples are defined as described in §2.1. While the mean M_B shows little dependence on environment for nearby blue galaxies, there is a much stronger dependence at $z \sim 1$.

ing lower in regions of higher overdensity. Again, this relationship is closely connected to the color–density relation, and so we would expect it to be weakened by the exclusion of the red–sequence population. In contrast, we find a stronger dependence of mean SFR on environment in DEEP2 when isolating the blue cloud than not. As detailed in §4, the relationship between SFR and galaxy density at $z \sim 1$ is a combination of two competing trends: the color–density relation and the dependence of mean luminosity on environment along the blue cloud. The inversion in the SFR–density relation at $z \sim 1$ relative to $z \sim 0$ is driven by the latter trend. Isolating the blue cloud effectively minimizes the role of the color–density relation, making the SFR–density relation monotonic.

5.2. The Impact of AGN Contamination

Another sensible reason for focusing solely on the blue–cloud population is to minimize the impact of contamination from active galactic nuclei (or AGN). As shown and discussed in detail by Yan et al. (2006), $[\text{O II}] \lambda 3727\text{\AA}$ emission is not a direct indicator of star formation in the local Universe. AGN, especially LINERs (Heckman 1980), can contribute significantly to the integrated $[\text{O II}]$ emission from nearby galaxies. This additional source of emission causes the measured SFR derived from $[\text{O II}]$ line luminosities to be an overestimate of the true total SFR for some portion of the galaxy population. The impact of such AGN activity on the galaxy sample is greatest along the red sequence; where roughly 35–45% of nearby red galaxies exhibit signatures of AGN activity (Yan et al. 2006).

Yan et al. (2006) show that galaxies with significant AGN activity can be identified based on emission–line diagnostics (e.g., $[\text{O II}]/\text{H}\alpha$, $[\text{N II}]/\text{H}\alpha$, and $\text{H}\beta/[\text{O III}]$ line ratios), and therefore removed from the galaxy sample (see also Kewley et al. 2006). In the SDSS, we identify

galaxies with likely AGN contamination based on several line–ratio criteria:

$$[\text{N II}]/\text{H}\alpha > 0.6 \quad (4)$$

$$W_{[\text{O III}]} > 5 \cdot W_{\text{H}\alpha} - 7 \quad (5)$$

$$\log_{10}([\text{O III}]/\text{H}\beta) > 0.61 / [\log_{10}([\text{N II}]/\text{H}\alpha) - 0.05] + 1.3 \quad (6)$$

where W_x and x denote equivalent widths and line luminosities for a given line, respectively. Equation 4 is designed to select most LINERs and a majority of Seyferts, while equation 5 is effective at identifying nearly all LINERs. Finally, equation 6 is based on AGN–selection in the SDSS by Kauffmann et al. (2003), which is less sensitive to aperture effects related to the SDSS fibers and therefore more inclusive in selecting AGN than the criterion proposed by Kewley et al. (2001). Any source meeting any of these criteria is flagged as a likely AGN and subsequently removed from the galaxy sample. The union of these three selection criteria gives an extremely inclusive sample of AGN, with many AGN–star–forming composites also being removed from the main galaxy sample as AGN.

At $z \sim 0.1$, we conclude that contamination from AGN does not introduce any systematic bias that strongly impacts the observed relationships between star formation and environment. Table 4 lists the coefficients from linear–regression fits to the dependence of mean SFR (and sSFR) on local galaxy overdensity for the SDSS–A sample with the AGN population removed (but non–AGN red galaxies still retained). For this restricted galaxy sample, we find that the results detailed in §3 for the full SDSS galaxy sample persist, with mean SFR and mean sSFR decreasing in regions of higher galaxy density. The strength of the relationship between average sSFR and environment is weaker when the AGN population is removed, largely due to the significantly smaller number of red galaxies in the SDSS sample after removing AGN contamination (again, reflecting the fact that the concentration of red galaxies in overdense regions dominates the color–density relation).

At $z \sim 1$, $\text{H}\alpha$ is redshifted out of the optical window, and thus out of the spectral range probed by DEEP2. As a result, the $[\text{O II}]$ emission from AGN is more difficult to disentangle from star–formation activity in our higher–redshift galaxy sample. While at $0.74 \lesssim z \lesssim 0.83$ we are able to use $[\text{O II}]$, $\text{H}\beta$, and $[\text{O III}]$ line ratios to distinguish AGN–like emission (Yan et al. 2006, 2007), restricting to galaxies in such a small redshift window severely constricts the sample size at high redshift (< 3500 galaxies). For this small sample, we find no significant difference in the relationships between sSFR, SFR, and environment with those found in the full DEEP2–A sample (cf. Table 4). We note that the exclusion of AGN in DEEP2 is only effective at removing Seyfert and LINER–like AGN emission; transition objects (TOs) tend to have similar $[\text{O III}]/\text{H}\beta$ ratios to those of the star–forming galaxies. To confidently exclude transition objects, $[\text{N II}]/\text{H}\alpha$ line diagnostics are needed (Yan et al. 2007). However, transition objects comprise only a fraction of the AGN–like population (e.g., $\sim 10\%$ of red galaxies in the SDSS are TOs).

For these reasons, we are not able to definitively gauge the impact of AGN activity on our results at $z \sim 1$,

TABLE 4
FITS TO (s)SFR–DENSITY RELATIONS

Sample	sSFR–density fits				SFR–density fits				Subset Selected
	a_0	a_1	σ_{a_0}	σ_{a_1}	a_0	a_1	σ_{a_0}	σ_{a_1}	
DEEP2–A	-8.76	-0.023	0.013	0.021	1.03	0.068	0.003	0.005	only blue galaxies
DEEP2–A	-8.89	-0.047	0.035	0.053	0.79	0.046	0.006	0.010	with AGN removed
SDSS–A	-9.99	-0.038	0.023	0.034	-0.07	-0.007	0.004	0.006	only blue galaxies
SDSS–A	-10.13	-0.120	0.026	0.040	-0.79	-0.107	0.004	0.006	with AGN removed

NOTE. — We list the coefficients and 1σ uncertainties for the parameters of the linear-regression fits to the sSFR–density and SFR–density relations given by $\log_{10}(< \text{sSFR} >) = a_1 * \log_{10}(1 + \delta_3) + a_0$ (cf. Fig. 10 and Fig. 11), for subsamples of the SDSS–A and DEEP2–A galaxy samples selected (i) to isolate the blue cloud and (ii) to remove AGN. For details of these selections, refer to §5.1 and §5.2.

other than to show it should not dominate the observed trends. As previously discussed, the contribution of AGN–related emission to [O II] line luminosities produces overestimated SFRs. However, as shown by Nandra et al. (2007) from X–ray observations of the Extended Groth Strip, most AGN at $z \sim 1$ are either along the red sequence or in between the red sequence and blue cloud, similar to what has been observed locally (Yan et al. 2006, 2007). When we restrict to just galaxies in the blue cloud within DEEP2, the inversion in the local SFR–density relation still persists, with SFR increasing in regions of higher density at $z \sim 1$; AGN cannot be driving this inversion.

In addition, spectroscopically–identified AGN comprise only a small portion ($< 5\%$) of the DEEP2 sample at moderate to high star–formation rates ($\text{SFR} > 10 \text{ M}_\odot/\text{yr}$). As such, AGN cannot be responsible for the rise in mean overdensity at high SFRs in Figure 12. Instead, AGN contamination would cause the U–shaped trend in Fig. 12 to be flattened, as red galaxies with no star–formation activity (which preferentially reside in regions of high galaxy density) would be placed into the range $0.25 < \log_{10}(\text{SFR}) < 1$ due to misaccounting of their AGN activity. Thus, we conclude that AGN contamination in the DEEP2 data set is not a viable explanation for the observed inversion in the SFR–density relation at $z \sim 1$.

Still, the impact of AGN contamination is clearly a concern when studying star formation at higher redshift, especially given the higher number density of AGN (both low– and high–luminosity) at $z \sim 1$ relative to what is found at $z \sim 0$ (e.g., Cowie et al. 2003; Hasinger 2003; Barger & Cowie 2005). A more detailed treatment of the role of AGN in DEEP2 will be included in future works using the multiwavelength data in the EGS (Yan et al. 2007; Woo et al. 2007; Marcillac et al. 2007; Georgakakis et al. 2007).

5.3. The Role of Dust

In contrast to AGN activity, which can lead to over–inflated SFR estimates, dust will cause some fraction of star formation to be hidden at optical or UV wavelengths, yielding a measurement of the total SFR that is an underestimate of the true SFR. To account for this effect, we have corrected our SFRs according to the mean relations of Moustakas et al. (2006), which calibrate SFRs derived from [O II] line luminosities against more precise SFR indicators (e.g., extinction–corrected $\text{H}\alpha$ –derived SFRs) from multiwavelength data; they find it is possible to

produce a correction which is a function only of galaxy luminosity, M_B , that accounts for both mean metallicity and reddening effects. While Moustakas et al. (2006) conclude that there remains significant scatter between these [O II]–derived SFR estimates and cleaner measures of star formation (at a level of roughly $\pm 90\%$), this lack of precision in our star–formation rates is not the dominant source of error in our analysis. Measures of galaxy environment are by nature imprecise, with a level of uncertainty dependent upon the sampling density and redshift precision and accuracy of the redshift survey. The errors in overdensity measures are the greatest obstacle to detecting trends between galaxy properties and environment at $z \sim 1$ and at $z \sim 0$. By applying the corrections of Moustakas et al. (2006), we should be able to reduce any overall bias in our analysis due to the use of [O II] as a SFR indicator to a modest level.

While the empirical calibrations of Moustakas et al. (2006) were derived from data at $z \sim 0$, they have been tested at higher redshifts (to $z \lesssim 1.4$), with no dependence on redshift observed. Still, the DEEP2 sample employed here probes fainter luminosities than the samples used by Moustakas et al. (2006) at $z > 0.7$. To test the sensitivity of our results to the particular calibration of the [O II]–derived star–formation rates at $z \sim 1$, we have redone our analysis with star–formation rate calibrations having $1/2\times$ or $2\times$ the luminosity–dependence given in Table 2 of Moustakas et al. (2006), accounting for a wide range in evolution of possible dust and metallicity effects. Even when we vary the luminosity–dependence of the [O II]/SFR calibration to such a degree, the form of the trends between both specific and total star–formation rate and environment at $z \sim 1$ remain similar (e.g., the SFR–density relation is still inverted relative to that found at $z \sim 0$, and the U–shaped dependence of average overdensity on SFR persists). We note that the *amplitude* of this calibration, rather than the strength of its luminosity–dependence, will not affect the conclusions of any of our studies at constant redshift, but only comparisons of the overall strength of star–formation at $z \sim 1$ to $z \sim 0.1$.

Clearly, if a source is sufficiently highly obscured, then we may detect no [O II] emission in the DEEP2 spectra. For such sources, the empirical calibrations of Moustakas et al. (2006) will not be appropriate. However, multiwavelength studies of star formation at $z \lesssim 3$ have shown that extinction is well–correlated with star–formation rate (Hopkins et al. 2001). As such, correcting for extinction beyond that expected from

Moustakas et al. (2006) would be expected to increase the strength of the trends observed in the DEEP2 sample, causing the average SFR to be yet higher in overdense regions.

One method for detecting heavily obscured sources and minimizing the impact of dust on SFR measurements is to observe at longer wavelengths (e.g., at $24\mu\text{m}$), where dust obscuration is much weaker. Analysis of the relationship between star formation and environment using *Spitzer*/MIPS data will be the subject of future papers (Marcillac et al. 2007; Woo et al. 2007) and will be a critical check to the results presented here. However, extremely deep infrared data is needed to include sources with star-formation rates as low as those measurable in the DEEP2 spectroscopy. For instance, within the EGS, 5421 of the DEEP2 sources are in the *Spitzer*/MIPS region, but only 1645 have $24\mu\text{m}$ detections to a flux limit of $S \sim 83\text{mJy}$ (Weiner et al. 2007). Ongoing, extremely deep *Spitzer*/MIPS observations in the EGS and the Extended Chandra Deep Field South (ECDFS) will provide data sets well-suited to future analyses of obscured star formation at intermediate redshift.

We note that although they do not appear to influence our environment results, the effects of dust extinction and AGN contamination may be responsible for the difference in the curvature of the isocontours of mean SFR as a function of color and absolute magnitude in the SDSS and DEEP2 samples, as seen in Figure 16. The higher number density of AGN at $z \sim 1$ relative to $z \sim 1$, especially on the red edge of the blue cloud and on the red sequence, inflates the mean SFR at those portions of the color-magnitude diagrams, thereby stretching the isocontours of mean SFR to redder colors. Similarly, the higher fraction of obscured star formation at intermediate redshift (Le Floc'h et al. 2005) could be responsible for elongating the isocontours at $z \sim 1$ with respect to those at $z \sim 0$.

6. THE ROLE OF ENVIRONMENT IN THE COSMIC SFH

As discussed in §1, one explanation which has been posited for the dramatic drop in the cosmic star-formation rate space density at $z < 1$ is a corresponding steep decline in the galaxy merger rate, which thereby reduces the amount of merger-induced star formation. Mergers of dark matter halos are integral to hierarchical structure formation; their rate may be calculated straightforwardly in the Extended Press-Schechter formalism (Press & Schechter 1974; Lacey & Cole 1993). Unfortunately, attempts to constrain the evolution in the galaxy merger rate through observations at $z < 1$, have produced mixed results.

Early imaging studies of galaxies at intermediate redshift using the *Hubble Space Telescope* (*HST*) found galaxies with disturbed morphologies (i.e., mergers) to be much more common at $z \sim 1$ than locally and attributed the rapid decline in the blue luminosity density to the evolution of this population (e.g., Abraham et al. 1996; Brinchmann et al. 1998; van den Bergh et al. 2000). In agreement with this finding, some estimates of the galaxy merger rate at $z < 1$ derived from analyses of galaxy morphologies and from studies of spectroscopic pairs, have found a significant decline in the frequency of major mergers over the last 7 Gyr (Zepf & Koo 1989; Patton et al. 1997; Le Fèvre et al. 2000; Conselice et al.

2003; Hammer et al. 2005; Kampczyk et al. 2007).

However, a number of other efforts to study galaxies at $z \sim 1$ have found a much more gradual decline in the pair fraction and merger rate since $z \sim 1$, downplaying the role of galaxy interactions in the evolution of the cosmic star-formation history (e.g., Neuschaefer et al. 1997; Carlberg et al. 2000; Bundy et al. 2004; Lin et al. 2004; Lotz et al. 2007). The abundance of contrasting results is, at least in part, due to the difficulty in measuring the merger rate, which depends significantly on the treatment of projection effects and assumptions regarding the timescales over which merger signatures are visible. Furthermore, despite having large differences in the best-fit rate, many of the seemingly-contradictory evolution estimates are still consistent with each other due to small sample sizes and large random errors. Many systematic problems could affect one method or another; for instance, Bell et al. (2006) argues that some of the variance in results is attributable to accounting errors in converting pair fractions into merger rates.

Recent studies at intermediate redshift have benefited from significantly larger sample sizes and deeper *HST* imaging over wider fields. While this has not yielded consensus on the evolution of the merger rate, studies of galaxy morphologies using data sets in fields such as the EGS and the ECDFS have found that the contribution from irregular (or peculiar) galaxies to the blue luminosity density to be subdominant at $z \sim 1$; for instance, results from Conselice et al. (2005), Wolf et al. (2005), and Zamojski et al. (2007) all indicate that the drop in the global SFR at $z < 1$ (as traced by the *B*-band and UV luminosity densities) is driven by a decline in the emission from galaxies with regular (i.e., non-disturbed) morphologies. Thus, regardless of the evolution in the merger rate, galaxy mergers must not be the dominant cause of the stark (~ 10 – $20\times$, Fukugita & Kawasaki 2003; Hopkins & Beacom 2006) decline in the global star-formation rate since $z \sim 1$.

This conclusion is supported by a variety of other galaxy studies at $z < 1$. Lin et al. (2007) placed an upper limit of $< 40\%$ on the contribution from galaxy pairs (i.e., precursors to mergers) to $24\mu\text{m}$ infrared emission at intermediate redshift. Similarly, Bell et al. (2005) find that the relationship between galaxy morphology and star-formation activity at $z \sim 0.7$ implies that major mergers (and the evolution in the major merger rate) cannot be the proximate cause of the decline in the cosmic star-formation rate. In agreement with these observational results, theoretical models of galaxy mergers predict that such interactions contribute only a small fraction of the total star-formation rate space density of the Universe (Hopkins et al. 2006).

Since galaxy mergers do not appear to be driving the global decline in the cosmic star-formation rate since $z < 1$, a new paradigm is required. Several multiwavelength studies of star formation at intermediate and low redshifts have concluded that the reduction in the global star-formation rate space density is largely driven by long-term processes such as gradual gas depletion, rather than galaxy mergers. For instance, Bauer et al. (2005) and (Noeske et al. 2007b) find that star-forming galaxies populate a tight sequence in SFR and stellar mass at $z < 1.2$, with a limited range in SFR at a given stellar mass and redshift (Noeske et al. 2007b). This con-

strains the amount of episodic star-formation activity that may be occurring, and indicates that star formation at $z < 1$ appears to be dominated by a gradual decline in the average SFR among the star-forming galaxy population. Strong, outlier bursts indicative of being driven by merger activity are rare, even at $z > 1$ (Noeske et al. 2007a).

While mergers (and environment) should play some role in the decline of the global SFR even if there is only a weak evolution in the merger rate, the growing consensus appears to be that mergers have relatively little effect on the global decline in star formation from $z \sim 1$ to $z \sim 0$. The impact of other environment-dependent mechanisms, however, could be significant. For instance, virial shock-heating of infalling gas onto massive dark matter halos can produce a smooth decline in star formation with time: as the flow of cold gas to galaxies in such halos is suspended, the galaxies suffer from starvation and gradually stop forming stars. Given the strong correlation between halo mass and local galaxy density (e.g., Lemson & Kauffmann 1999; Gao et al. 2004; Wetzel et al. 2007; Croton et al. 2007), this process should exhibit a close connection with galaxy environment. Similarly, conductive heating of gas can halt star formation within infalling galaxies onto a cluster or group (Cowie & McKee 1977; Cowie & Songaila 1977). Like ram-pressure stripping, evaporation occurs most efficiently in the central regions of clusters. However, the gas density and temperature in the outskirts of clusters or in groups are sufficient to make these processes efficient in less extreme environs than the centers of the most massive clusters (Fujita & Goto 2004; Hester 2006).

However, the results of this paper show that environment-dependent (or environment-related) processes are not responsible for driving the decline in the cosmic star-formation rate. Instead, our analysis supports the general picture of a smooth decline in the typical galaxy SFR, with only a relatively minor impact from environment-related mechanisms such as mergers, evaporation associated with conductive heating, and ram-pressure stripping. The star-formation rate in both dense and underdense regions has decreased rapidly since $z \sim 1$, rather than primarily declining in group and cluster-like environments.

Figure 18 shows the decline in the average (and median) SFR for the blue galaxy population within the volume-limited [relative to $M_B^*(z)$] DEEP2-C and SDSS-B samples. The evolution in the mean SFR is much stronger than the dependence of mean SFR on environment at $z \sim 1$ or $z \sim 0$ (cf. Fig. 11); the average (or median) SFR drops by a factor of ~ 20 between $z \sim 1$ and $z \sim 0.1$, while the contrast between the mean SFR in the highest- and lowest-density regions is less than a factor 2 at both $z \sim 1$ and $z \sim 0.1$. Changing the rate of M_B^* evolution used to define these samples (i.e., the parameter Q in Equation 2) changes these results only modestly; the growth in the mean SFR for these matched samples ranges from a factor of ~ 18 to ~ 16 for $Q = -1.37$ or $Q = -1$. While our results show that environment is clearly correlated with star-formation activity at $z < 1$ and that there is significant evolution in the relationship between mean SFR and galaxy overdensity from $z \sim 1$ to $z \sim 0$, the strength of the SFR-density

relation and its evolution at $z < 1$ is a small perturbation on the overall decline in the global star-formation rate space density. If environment-related processes played a dominant role in the cosmic star-formation history over the last 7 Gyr, then we would expect the decline of the cosmic star formation rate to be associated with only a subset of environments.

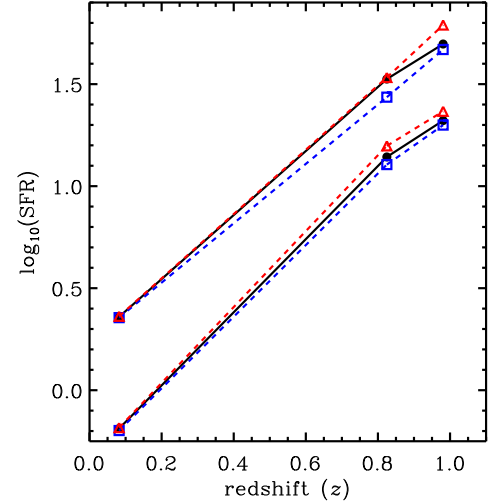


FIG. 18.— The mean and median galaxy SFR as a function of redshift for blue galaxies in the SDSS-B and DEEP2-C samples (black filled circles). The blue galaxy populations are selected according to Equation 1, with an offset of 0.14 magnitudes for the SDSS as described in §2.1). The DEEP2-C sample is divided into two sub-samples according to redshift ($0.75 < z < 0.9$ and $0.9 < z < 1.05$). The blue squares and red triangles show the evolution in the mean and median SFR for blue galaxies in the lowest-density (bottom 20%, blue squares) and highest-density (top 20%, red triangles) environments in the corresponding redshift regime. Note that the values tracing the evolution in the mean SFR are offset by +0.25 in $\log_{10}(\text{SFR})$ to facilitate display. The overall decline in the mean and median SFR with redshift is significantly greater than the dependence of the mean and median SFR on environment at either $z \sim 0$ or $z \sim 1$. Note that the star-formation rates are given in units of $h^{-2} M_{\odot}/\text{yr}$.

While galaxy environment does not dictate the evolution of the global star-formation activity at $z < 1$, it does play a central role in both the complete quenching of star formation (i.e., the creation of “red and dead” galaxies) and the evolution of the bright, blue galaxy (BBG) population. As first shown by Cooper et al. (2006), all major features of the color-density relation were in place by $z \sim 1$. This significant relationship between rest-frame color and environment, which is echoed in the sSFR-density relation, is a result of star-formation activity being completely halted in groups much more frequently than in less-dense environments. Similarly, by analyzing the evolution of the blue galaxy fraction in both galaxy groups and the field in DEEP2, Gerke et al. (2007) showed that the growth in the abundance of galaxies on the red sequence (e.g., Brown et al. 2007; Faber et al. 2007) occurred primarily in groups and clusters of galaxies at $z < 1.3$ (see also Cooper et al. 2007).

Environment plays a related role in the evolution of BBGs. As first discussed by Cooper et al. (2006), in order to reconcile the differences in the luminosity-environment trends at $z \sim 1$ and $z \sim 0$, the BBGs in

dense environments at $z \sim 1$ must have ceased star formation and moved onto the red sequence by the present epoch. This evolution may play a significant role in the evolution of the bright end of the blue galaxy luminosity function, which sees a significant drop off in number density at bright magnitudes over the last 7 Gyr (e.g., Willmer et al. 2006; Bundy et al. 2006; Zucca et al. 2006). This quenching of the BBGs in overdense environments will have only a small impact on the global SFR, as the most massive galaxies contribute only a small portion of the total SFR density at $z < 1$ (Juneau et al. 2005; Zheng et al. 2007).

As this paper was being completed, a parallel analysis of the relationship between star formation and environment at intermediate redshift was presented by Elbaz et al. (2007). Our results, which are based on a significantly larger sample and probe to lower levels of star-formation activity, are in relatively good agreement with those of Elbaz et al. (2007). Both analyses find an inversion (or “reversal”) in the SFR–density relation at $z \sim 1$ relative to the local relation. Furthermore, both studies conclude that major mergers cannot be the solitary physical mechanism responsible for the correlation between SFR and galaxy overdensity at intermediate redshift. Using *HST*/ACS imaging data, Elbaz et al. (2007) conclude that the majority of luminous infrared galaxies in high-density regions at $z \sim 1$ exhibit normal spiral morphologies — i.e., they are not disturbed systems showing signatures of recent mergers (see also Melbourne et al. 2005).

The Elbaz et al. (2007) data set, which is based on deep $24\mu\text{m}$ *Spitzer*/MIPS imaging in the GOODS (Dickinson et al. 2003) fields, provides a reassuring cross-check to our study based on [O II] line luminosities. While multiwavelength analysis in the ECDFS, GOODS, and EGS fields (e.g., Marcillac et al. 2007; Woo et al. 2007) will further explore the impact of dust and metallicity on the connection between environment and star formation at $z < 1$, the agreement between our work and that of Elbaz et al. (2007) indicates that extinction effects are not strongly biasing our results at $z \sim 1$, and that missing low-SFR galaxies is not dominating their results.

7. SUMMARY & CONCLUSIONS

In this paper, we present a detailed study of the relationship between star formation and local environment at both $z \sim 0$ and $z \sim 1$ using galaxy samples drawn from the SDSS and DEEP2 surveys. We estimate the local overdensity about each galaxy according to the projected 3rd-nearest-neighbor surface density, and measure star-formation rates using [O II] $\lambda 3727\text{\AA}$ line luminosities, calibrated to more robust star-formation indicators. Our principal results are as follows:

- We find that the relationships between specific

star-formation rate and environment at $z \sim 0$ and at $z \sim 1$ are very similar, with the mean sSFR decreasing in regions of higher galaxy density. We conclude that this trend, like the color–density relation at $z < 1$, is driven by the quenching of star formation in regions of high galaxy overdensity (i.e., galaxy groups and clusters). At both epochs, we find a close correlation between sSFR and rest-frame $U - B$ color.

- In contrast to the local SFR–density relation, we find an inversion in the dependence of mean SFR on local overdensity at $z \sim 1$, such that the typical SFR increases in higher-density regions, rather than decreasing as at $z \sim 0$. At $z \sim 1$, both the highest- and lowest-SFR galaxies are typically found in denser regions than intermediate objects, while at $z \sim 0$, the highest-SFR galaxies prefer void-like environments. This reflects the fact that there is a significant positive correlation between luminosity and overdensity at $z \sim 1$ which is weak or absent locally. These trends are associated with the existence a population of bright, massive blue galaxies in dense regions at $z \sim 1$, as first discovered by Cooper et al. (2006), which have no local counterparts. This galaxy population is thought to evolve into members of the red sequence from $z \sim 1$ to $z \sim 0$.
- Environmental effects do not play a dominant role in shaping the cosmic star-formation history at $z < 1$. The dependence of the mean galaxy SFR on local galaxy density and its evolution from $z \sim 1$ to $z \sim 0$ is much weaker than the decline in the global SFR space density over the last 7 Gyr.

This work was supported in part by NSF grants AST-0071048 AST-0071198, AST-0507428, and AST-0507483 as well as Hubble Space Telescope Archival grant, HST-AR-10947.01. A.L.C. acknowledges support by NASA through Hubble Fellowship grant HST-HF-01182.01-A, awarded by the Space Telescope Science Institute, which is operated by AURA Inc. under NASA contract NAS 5-26555. M.C.C. would like to thank Greg Wirth and all of the Keck Observatory staff for their help in the acquisition of the Keck/DEIMOS data. M.C.C. would also like to thank Michael Blanton and David Hogg for their assistance in utilizing the NYU-VAGC data products.

We also wish to recognize and acknowledge the highly significant cultural role and reverence that the summit of Mauna Kea has always had within the indigenous Hawaiian community. It is a privilege to be given the opportunity to conduct observations from this mountain.

REFERENCES

- Abraham, R. G., van den Bergh, S., Glazebrook, K., Ellis, R. S., Santiago, B. X., Surma, P., & Griffiths, R. E. 1996, ApJS, 107, 1
- Adelman-McCarthy, J. K. et al. 2006, ApJS, 162, 38
- Baldry, I. K., Balogh, M. L., Bower, R. G., Glazebrook, K., Nichol, R. C., Bamford, S. P., & Budavari, T. 2006, MNRAS, 373, 469
- Balogh, M. et al. 2004a, MNRAS, 348, 1355
- Balogh, M. L., Baldry, I. K., Nichol, R., Miller, C., Bower, R., & Glazebrook, K. 2004b, ApJ, 615, L101

- Balogh, M. L., Schade, D., Morris, S. L., Yee, H. K. C., Carlberg, R. G., & Ellingson, E. 1998, *ApJ*, 504, L75+
- Barger, A. J. & Cowie, L. L. 2005, *ApJ*, 635, 115
- Bauer, A. E., Drory, N., Hill, G. J., & Feulner, G. 2005, *ApJ*, 621, L89
- Bell, E. F., McIntosh, D. H., Katz, N., & Weinberg, M. D. 2003, *ApJS*, 149, 289
- Bell, E. F., Phleps, S., Somerville, R. S., Wolf, C., Borch, A., & Meisenheimer, K. 2006, *ApJ*, 652, 270
- Bell, E. F. et al. 2004, *ApJ*, 608, 752
- . 2005, *ApJ*, 625, 23
- Birnboim, Y. & Dekel, A. 2003, *MNRAS*, 345, 349
- Blanton, M. R. 2006, *ApJ*, 648, 268
- Blanton, M. R., Eisenstein, D., Hogg, D. W., Schlegel, D. J., & Brinkmann, J. 2005a, *ApJ*, 629, 143
- Blanton, M. R., Eisenstein, D., Hogg, D. W., & Zehavi, I. 2006, *ApJ*, 645, 977
- Blanton, M. R. & Roweis, S. 2007, *AJ*, 133, 734
- Blanton, M. R. et al. 2003, *AJ*, 125, 2348
- . 2005b, *AJ*, 129, 2562
- Brinchmann, J. et al. 1998, *ApJ*, 499, 112
- Brown, M. J. I., Dey, A., Jannuzi, B. T., Brand, K., Benson, A. J., Brodwin, M., Croton, D. J., & Eisenhardt, P. R. 2007, *ApJ*, 654, 858
- Bruzual, G. & Charlot, S. 2003, *MNRAS*, 344, 1000
- Bundy, K., Ellis, R. S., & Conselice, C. J. 2005, *ApJ*, 625, 621
- Bundy, K., Fukugita, M., Ellis, R. S., Kodama, T., & Conselice, C. J. 2004, *ApJ*, 601, L123
- Bundy, K. et al. 2006, *ApJ*, 651, 120
- Carlberg, R. G. et al. 2000, *ApJ*, 532, L1
- Cassata, P. et al. 2007, *ApJS*, submitted [astro-ph/0701483]
- Cavaliere, A., Colafrancesco, S., & Menci, N. 1992, *ApJ*, 392, 41
- Chabrier, G. 2003, *PASP*, 115, 763
- Christlein, D. & Zabludoff, A. I. 2005, *ApJ*, 621, 201
- Coil, A. L., Newman, J. A., Cooper, M. C., Davis, M., Faber, S. M., Koo, D. C., & Willmer, C. N. A. 2006, *ApJ*, 644, 671
- Coil, A. L., Newman, J. A., Kaiser, N., Davis, M., Ma, C.-P., Kocevski, D. D., & Koo, D. C. 2004a, *ApJ*, 617, 765
- Coil, A. L. et al. 2004b, *ApJ*, 609, 525
- Colless, M. et al. 2001, *MNRAS*, 328, 1039
- Conselice, C. J., Bershad, M. A., Dickinson, M., & Papovich, C. 2003, *AJ*, 126, 1183
- Conselice, C. J., Blackburne, J. A., & Papovich, C. 2005, *ApJ*, 620, 564
- Cooper, M. C., Newman, J. A., Madgwick, D. S., Gerke, B. F., Yan, R., & Davis, M. 2005, *ApJ*, 634, 833
- Cooper, M. C. et al. 2006, *MNRAS*, 370, 198
- . 2007, *MNRAS*, 376, 1445
- Cowie, L. L., Barger, A. J., Bautz, M. W., Brandt, W. N., & Garmire, G. P. 2003, *ApJ*, 584, L57
- Cowie, L. L. & McKee, C. F. 1977, *ApJ*, 211, 135
- Cowie, L. L. & Songaila, A. 1977, *Nature*, 266, 501
- Cox, T. J., Jonsson, P., Primack, J. R., & Somerville, R. S. 2006, *MNRAS*, 373, 1013
- Croton, D. J., Gao, L., & White, S. D. M. 2007, *MNRAS*, 374, 1303
- Cucciati, O. et al. 2006
- Davis, M. & Geller, M. J. 1976, *ApJ*, 208, 13
- Davis, M. et al. 2003, in *Discoveries and Research Prospects from 6- to 10-Meter-Class Telescopes II*. Edited by Guhathakurta, Puragra. Proceedings of the SPIE, Volume 4834, pp. 161-172 (2003), 161-172
- Davis, M. et al. 2007, *ApJ*, 660, L1
- Dickinson, M., Giavalisco, M., & The GOODS Team. 2003, in *The Mass of Galaxies at Low and High Redshift*, ed. R. Bender & A. Renzini, 324+
- Elbaz, D. et al. 2007, *A&A*, submitted [astro-ph/0703653]
- Faber, S. M. et al. 2007, *ApJ*, accepted [astro-ph/0506044]
- . 2008, 2008, in prep
- Fujita, Y. & Goto, T. 2004, *PASJ*, 56, 621
- Fukugita, M. & Kawasaki, M. 2003, *MNRAS*, 340, L7
- Gómez, P. L. et al. 2003, *ApJ*, 584, 210
- Gao, L., White, S. D. M., Jenkins, A., Stoehr, F., & Springel, V. 2004, *MNRAS*, 355, 819
- Georgakakis, A. et al. 2007, *MNRAS*, in prep
- Gerke, B. F. et al. 2005, *ApJ*, 625, 6
- . 2007, *MNRAS*, 376, 1425
- Gunn, J. E. & Gott, J. R. I. 1972, *ApJ*, 176, 1
- Hammer, F., Flores, H., Elbaz, D., Zheng, X. Z., Liang, Y. C., & Cesarsky, C. 2005, *A&A*, 430, 115
- Hasinger, G. 2003, in *AIP Conf. Proc. 666: The Emergence of Cosmic Structure*, ed. S. H. Holt & C. S. Reynolds, 227-236
- Heckman, T. M. 1980, *A&A*, 87, 152
- Hester, J. A. 2006, *ApJ*, 647, 910
- Hogg, D. W. et al. 2003, *ApJ*, 585, L5
- . 2004, *ApJ*, 601, L29
- Hopkins, A. M. 2004, *ApJ*, 615, 209
- Hopkins, A. M. & Beacom, J. F. 2006, *ApJ*, 651, 142
- Hopkins, A. M., Connolly, A. J., Haarsma, D. B., & Cram, L. E. 2001, *AJ*, 122, 288
- Hopkins, P. F., Somerville, R. S., Hernquist, L., Cox, T. J., Robertson, B., & Li, Y. 2006, *ApJ*, 652, 864
- Juneau, S. et al. 2005, *ApJ*, 619, L135
- Kaiser, N. 1987, *MNRAS*, 227, 1
- Kampczyk, P. et al. 2007, *ApJS*, submitted [astro-ph/0611187]
- Kauffmann, G., White, S. D. M., Heckman, T. M., Ménard, B., Brinchmann, J., Charlot, S., Tremonti, C., & Brinkmann, J. 2004, *MNRAS*, 353, 713
- Kauffmann, G. et al. 2003, *MNRAS*, 346, 1055
- Kennicutt, Jr., R. C. 1998, *ARA&A*, 36, 189
- Kereš, D., Katz, N., Weinberg, D. H., & Davé, R. 2005, *MNRAS*, 363, 2
- Kewley, L. J., Dopita, M. A., Sutherland, R. S., Heisler, C. A., & Trevena, J. 2001, *ApJ*, 556, 121
- Kewley, L. J., Groves, B., Kauffmann, G., & Heckman, T. 2006, *MNRAS*, 372, 961
- Lacey, C. & Cole, S. 1993, *MNRAS*, 262, 627
- Le Fèvre, O. et al. 2000, *MNRAS*, 311, 565
- . 2005, *A&A*, 439, 845
- Le Floc'h, E. et al. 2005, *ApJ*, 632, 169
- Lemson, G. & Kauffmann, G. 1999, *MNRAS*, 302, 111
- Lewis, I. et al. 2002, *MNRAS*, 334, 673
- Lilly, S. J., Le Fèvre, O., Hammer, F., & Crampton, D. 1996, *ApJ*, 460, L1+
- Lin, L. et al. 2004, *ApJ*, 617, L9
- . 2007, *ApJ*, 660, L51
- Lotz, J. M. et al. 2007, *ApJ*, accepted [astro-ph/0602088]
- Madau, P., Ferguson, H. C., Dickinson, M. E., Giavalisco, M., Steidel, C. C., & Fruchter, A. 1996, *MNRAS*, 283, 1388
- Marcillac, D. et al. 2007, *ApJ*, in prep
- McCarthy, I. G. et al. 2007, *MNRAS*, 376, 497
- Melbourne, J., Koo, D. C., & Le Floc'h, E. 2005, *ApJ*, 632, L65
- Mihos, J. C. & Hernquist, L. 1996, *ApJ*, 464, 641
- Moore, B., Katz, N., Lake, G., Dressler, A., & Oemler, A. 1996, *Nature*, 379, 613
- Moore, B., Lake, G., & Katz, N. 1998, *ApJ*, 495, 139
- Moustakas, J., Kennicutt, Jr., R. C., & Tremonti, C. A. 2006, *ApJ*, 642, 775
- Nandra, K. et al. 2007, *ApJ*, 660, L11
- Neuschaefer, L. W., Im, M., Ratnatunga, K. U., Griffiths, R. E., & Casertano, S. 1997, *ApJ*, 480, 59
- Noeske, K. G. et al. 2007a, *ApJ*, 660, L47
- . 2007b, *ApJ*, 660, L43
- Nuijten, M. J. H. M., Simard, L., Gwyn, S., & Röttgering, H. J. A. 2005, *ApJ*, 626, L77
- Oke, J. B. & Gunn, J. E. 1983, *ApJ*, 266, 713
- Patton, D. R., Pritchet, C. J., Yee, H. K. C., Ellingson, E., & Carlberg, R. G. 1997, *ApJ*, 475, 29
- Press, W. H. & Schechter, P. 1974, *ApJ*, 187, 425
- Scoville, N. et al. 2007, *ApJS*, submitted [astro-ph/0612305]
- Steidel, C. C., Adelberger, K. L., Giavalisco, M., Dickinson, M., & Pettini, M. 1999, *ApJ*, 519, 1
- Tremonti, C. A. et al. 2004, *ApJ*, 613, 898
- van den Bergh, S., Cohen, J. G., Hogg, D. W., & Blandford, R. 2000, *AJ*, 120, 2190
- van Dokkum, P. G. & Franx, M. 2001, *ApJ*, 553, 90
- Vogt, N. P. et al. 2005, *ApJS*, 159, 41
- Weiner, B. J. et al. 2007, *ApJ*, 660, L39
- Weinmann, S. M., van den Bosch, F. C., Yang, X., & Mo, H. J. 2006, *MNRAS*, 366, 2
- Wetzel, A. R., Cohn, J. D., White, M., Holz, D. E., & Warren, M. S. 2007, *ApJ*, 656, 139
- Willmer, C. N. A. et al. 2006, *ApJ*, 647, 853

- Wilson, G., Cowie, L. L., Barger, A. J., & Burke, D. J. 2002, *AJ*, 124, 1258
- Wolf, C., Dye, S., Kleinheinrich, M., Meisenheimer, K., Rix, H.-W., & Wisotzki, L. 2001, *A&A*, 377, 442
- Wolf, C. et al. 2005, *ApJ*, 630, 771
- Woo, J. et al. 2007, *ApJ*, in prep
- Yan, R., Newman, J. A., Faber, S. M., Konidaris, N., Koo, D., & Davis, M. 2006, *ApJ*, 648, 281
- Yan, R. et al. 2007, *ApJ*, in prep
- York, D. G. et al. 2000, *AJ*, 120, 1579
- Zamojski, M. A. et al. 2007, *ApJS*, submitted
- Zehavi, I. et al. 2002, *ApJ*, 571, 172
- . 2005, *ApJ*, 630, 1
- Zepf, S. E. & Koo, D. C. 1989, *ApJ*, 337, 34
- Zheng, X. Z., Bell, E. F., Papovich, C., Wolf, C., Meisenheimer, K., Rix, H.-W., Rieke, G. H., & Somerville, R. 2007, *ApJ*, submitted [astro-ph/0702208]
- Zucca, E. et al. 2006, *A&A*, 455, 879